The Astrophysical Journal, 961:73 (30pp), 2024 January 20 https://doi.org/10.3847/1538-4357/ad0966

Outshining by Recent Star Formation Prevents the Accurate Measurement of High-z Galaxy Stellar Masses

Desika Narayanan[1,2], Sidney Lower[1], Paul Torrey[1], Gabriel Brammer[2], Weiguang Cui[3,4,5], Romeel Davé[5,6], Kartheik G. Iyer[7,15], Qi Li[8], Christopher C. Lovell[9,10], Laura V. Sales[11], Daniel P. Stark[12], Federico Marinacci[13], and Mark Vogelsberger[14]

[1] Department of Astronomy, University of Florida, 211 Bryant Space Sciences Center, Gainesville, FL 32611, USA; desika.narayanan@ufl.edu
[2] Cosmic Dawn Center (DAWN), Niels Bohr Institute, University of Copenhagen, Jagtvej 128, København N, DK-2200, Denmark
[3] Departamento de Física Teórica, M-8, Universidad Autónoma de Madrid, Cantoblanco E-28049, Madrid, Spain
[4] Centro de Investigación Avanzada en Física Fundamental (CIAFF), Universidad Autónoma de Madrid, Cantoblanco, E-28049 Madrid, Spain
[5] Institute for Astronomy, University of Edinburgh, Royal Observatory, Edinburgh EH9 3HJ, UK
[6] Department of Physics and Astronomy, University of the Western Cape, Bellville, Cape Town 7535, South Africa
[7] Columbia Astrophysics Laboratory, Columbia University, 550 West 120th Street, New York, NY 10027, USA
[8] Max Planck Institute for Astrophysics, Garching bei Munchen, Germany
[9] Institute of Cosmology and Gravitation, University of Portsmouth, Burnaby Road, Portsmouth PO1 3FX, UK
[10] Astronomy Centre, University of Sussex, Falmer, Brighton BN1 9QH, UK
[11] Department of Physics and Astronomy, University of California, Riverside, CA 92521, USA
[12] Steward Observatory, University of Arizona, 933 N. Cherry Avenue, Tucson, AZ 85721, USA
[13] Department of Physics & Astronomy "Augusto Righi," University of Bologna, via Gobetti 93/2, I-40129 Bologna, Italy
[14] Department of Physics, Kavli Institute for Astrophysics and Space Research, Massachusetts Institute of Technology, Cambridge, MA 02139, USA
Received 2023 June 15; revised 2023 October 31; accepted 2023 November 1; published 2024 January 16

Abstract

We demonstrate that the inference of galaxy stellar masses via spectral energy distribution (SED) fitting techniques for galaxies formed in the first billion years after the Big Bang carries fundamental uncertainties owing to the loss of star formation history (SFH) information from the very first episodes of star formation in the integrated spectra of galaxies. While this early star formation can contribute substantially to the total stellar mass of high-redshift systems, ongoing star formation at the time of detection outshines the residual light from earlier bursts, hampering the determination of accurate stellar masses. As a result, order-of-magnitude uncertainties in stellar masses can be expected. We demonstrate this potential problem via direct numerical simulation of galaxy formation in a cosmological context. In detail, we carry out two cosmological simulations with significantly different stellar feedback models, which span a significant range in SFH burstiness. We compute the mock SEDs for these model galaxies at $z = 7$ via calculations of 3D dust radiative transfer, and then backward fit these SEDs with PROSPECTOR SED fitting software. The uncertainties in derived stellar masses that we find for $z > 7$ galaxies motivate the development of new techniques and/or priors for SFH to model star formation in the early Universe.

Unified Astronomy Thesaurus concepts: Galaxies (573); Galaxy ages (576); High-redshift galaxies (734); Starburst galaxies (1570)

1. Introduction

The most common method for determining the stellar mass of a galaxy is through ultraviolet–near-infrared spectral energy distribution (SED) modeling. This technique, first developed by Tinsley (1968), Spinrad & Taylor (1971), and Faber (1972), models the expected emission from stellar populations as they evolve over an assumed star formation history (SFH), with the emission reddened by a wavelength-dependent dust attenuation curve (see Walcher et al. 2011; Conroy & van Dokkum 2012; Salim & Narayanan 2020; Pacifici et al. 2023, for reviews). This powerful technique is foundational for our current observational understanding of the cosmic evolution of star formation rates and stellar masses in galaxies (e.g., Madau & Dickinson 2014), and indeed a diverse range of methodologies for SED fitting have been explored in recent years (Brammer et al. 2008; da Cunha et al. 2008; Kriek et al. 2009; Chevallard & Charlot 2016; Iyer & Gawiser 2017; Carnall et al. 2018; Johnson et al. 2021).

The assumed form for the model SFH in SED fitting software is an essential element in deriving galaxy stellar masses. Traditional functional forms for the SFH include constant, exponential declining, and burst models, and combinations of these among others (Conroy 2013). These parameterized forms for SFH (hereafter, "parametric" SFHs) have parameters describing the (for example) normalization, e-folding time, and amplitude of bursts that are varied until a match is found between the synthetic SED produced by the stellar population synthesis model and the observed data. When a solution is found, the model SFH is then used to infer the stellar mass of the observed galaxy (typically assuming a fixed metallicity). Of course, the assumed form of this SFH can severely impact the modeled stellar mass (Michalowski et al. 2012; Simha et al. 2014; Acquaviva et al. 2015; Iyer & Gawiser 2017; Carnall et al. 2018, 2019; Dudzevičiūtė et al. 2020).

More recently, a number of codes have explored the impact of more flexible so-called "nonparametric" forms for the model SFH (e.g., Heavens et al. 2000; Tojeiro et al. 2007; Iyer & Gawiser 2017; Johnson et al. 2021). Nonparametric SFH models do not have an explicit functional form like the

[15] Hubble Fellow.

parametric models, but instead can vary the amplitude of the SFH over a number of redshift or time bins in the modeled history of the galaxy. Iyer et al. (2018) validated the usage of nonparametric SFHs constructed via Gaussian processes by ground-truthing these methods against the Santa Cruz semi-analytic model and the MUFASA cosmological simulation (Davé et al. 2016, 2017). Similarly, Lower et al. (2020) demonstrated the efficacy of nonparametric SFH techniques by ground-truthing modeled mock SEDs from galaxy simulations against their true stellar masses. Lower et al. (2020) found that while traditional parametric forms for the SFH in SED fitting software had uncertainties at the level ∼0.4 dex, nonparametric SFH models reduced these uncertainties to a level of ∼0.1 dex. Leja et al. (2019b) found that observed galaxies from the 3D-HST catalog (Brammer et al. 2012; Skelton et al. 2014) are systematically more massive and older when using nonparametric SFHs as compared to parametric methods, which bring the observed main sequence in line with theoretical predictions, potentially alleviating the long-standing tension between theory and observations in the star formation rate (SFR) of galaxies at $z \approx 2$ at a fixed stellar mass (Davé 2008; van Dokkum 2008).

With the successful launch of the JWST in 2021, observations are characterizing the physical properties of galaxies at unprecedented redshifts (e.g., Finkelstein et al. 2022a, 2022b; Castellano et al. 2022; Naidu et al. 2022; Adams et al. 2023; Atek et al. 2023; Donnan et al. 2023; Harikane et al. 2023; Labbé et al. 2023; Robertson et al. 2023). Beyond providing constraints on the buildup of stellar mass in some of the earliest galaxies in the Universe, JWST observations of high-redshift galaxies have been used to demonstrate potential tensions with the standard ΛCDM model (e.g., Lovell et al. 2019; Haslbauer et al. 2022; Boylan-Kolchin 2023; Labbé et al. 2023; Mason et al. 2023). What has yet to be explored, however, is the ability of traditional SED fitting methods to accurately derive stellar masses in these earliest galaxies, and particularly the problem of stellar "outshining."

The problem of stellar outshining refers to the light from recent bursts of star formation overwhelming that of older stellar populations, making the inference of their stellar masses difficult. The potential impact of outshining has a rich history in the observational literature. Papovich et al. (2001) demonstrated an uncertainty of ∼3–8 in the derived stellar masses of $z \sim 2$–3 Lyman break galaxies due to uncertainties in the modeling of SFH. This result has been further studied by Shapley et al. (2001, 2005), Daddi et al. (2004), Trager et al. (2008), Graves & Faber (2010), Sorba & Sawicki (2018), Tacchella et al. (2022), Topping et al. (2022), Whitler et al. (2023), and Giménez-Arteaga et al. (2023), among many other studies. From a theoretical standpoint, Maraston et al. (2010), Pforr et al. (2013), and Suess et al. (2022) constructed mock SFHs combined with stellar population modeling to study the potential impact of outshining.

The potential impact of stellar outshining by recent star formation on the inference of stellar mass has yet to be studied in bona fide cosmological hydrodynamic simulations of galaxy formation. In this paper, we use numerical simulations of galaxy formation, combined with postprocessed radiative transfer and SED fitting software, to study the impact of outshining on estimates of stellar mass in galaxies, with a particular emphasis on high-z galaxy detections by JWST. We demonstrate that standard SED fitting techniques have a difficult time deriving correct stellar masses in high-z galaxies owing to outshining by recent bursts of star formation. We find that early bursts of star formation can contribute significantly to the total stellar mass of a galaxy. By the time the galaxy is detected at relatively late times ($z \approx 7$–10), the current ongoing star formation outshines the light from evolved stars, making the integrated buildup of stellar mass difficult to measure. We demonstrate this effect using similar techniques to Lower et al. (2020)'s study of the efficacy of nonparametric SFH modeling: we simulate the formation of galaxies in cosmological simulations, forward model their mock SEDs using dust radiative transfer, and then fit these mock SEDs using standard techniques. This allows us to compare to ground truth from the simulations, and assess the efficacy of the fitting procedure.

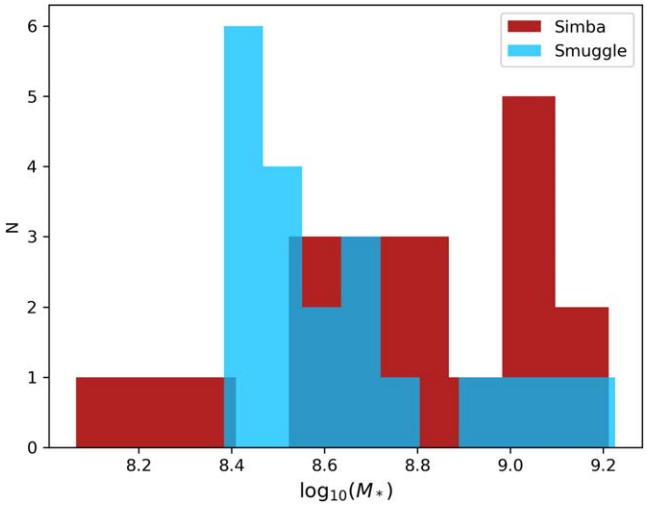

Figure 1. Histogram of the stellar masses at $z \sim 7.5$ for the 20 most massive galaxies in the SIMBA cosmological simulation (red) and the SMUGGLE cosmological box (blue). Both boxes are $25/h$ Mpc on a side.

In the remainder of this paper, we expand on these points. In Section 2, we describe our numerical methods; in Section 3, we describe the physical and luminous properties of the galaxies that we model; in Section 4, we demonstrate the main issues when SED fitting very young galaxies; in Section 5, we provide discussion, and in Section 6, we summarize our main results.

2. Methods

2.1. Summary of Methods

Our main goal is to create mock SEDs from galaxies formed in a cosmological simulation, and then fit those SEDs as an observer would in order to ground-truth SED fitting techniques for $z > 7$ galaxies. To do this, we first simulate the high-redshift evolution of galaxies by conducting cosmological hydrodynamic simulations of galaxy evolution. We then "forward model" the emission from these galaxies by coupling them with dust radiative transfer in order to generate their mock SEDs. With these SEDs in hand, we then "backward model" them in order to derive the inferred physical properties of the galaxies. Through this methodology, we determine the relationship between the stellar masses of our modeled galaxies inferred from their SEDs and the true stellar mass.

2.2. Simulations of Galaxy Formation

We employ two rather different cosmological galaxy formation models in order to ensure the robustness of our

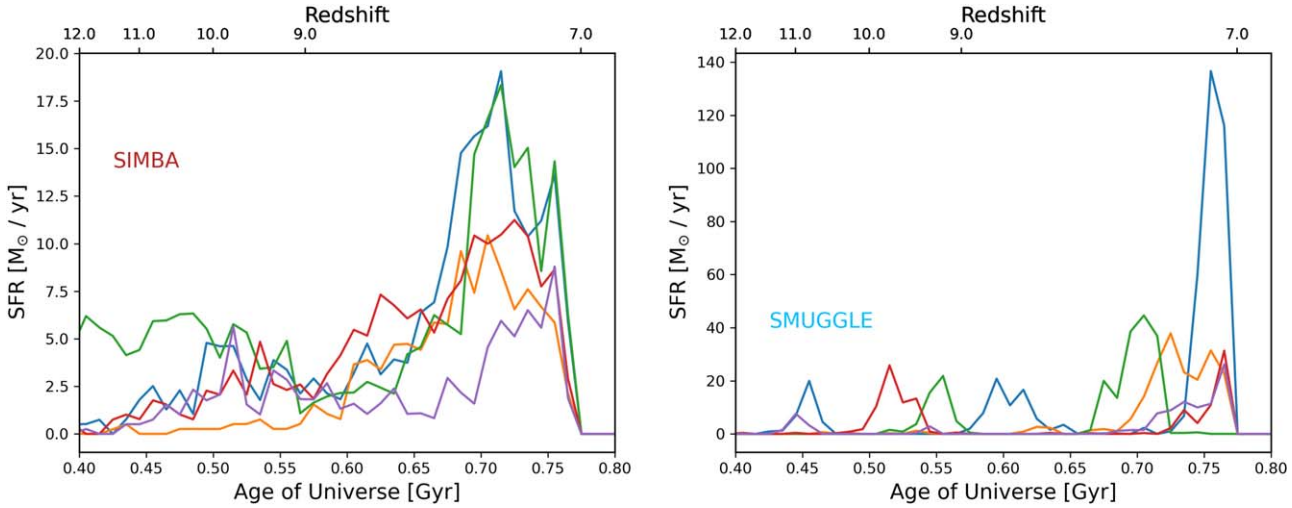

Figure 2. Example SFHs of five arbitrarily chosen galaxies from the SIMBA (left) and SMUGGLE (right) cosmological boxes. The former has an artificially pressurized ISM (as do most cosmological galaxy formation models), while the latter represents a class of explicit feedback models. The two models highlight the diversity of burstiness in modeled SFH that is possible in galaxy formation models. We use both of these models in our analysis to model a range of possibilities when investigating the efficacy of SED fitting in young galaxies. Note that the sudden drop-off in the SFH at $z < 7$ is an artifact of our constructing the SFHs at $z = 7$, and not physical.

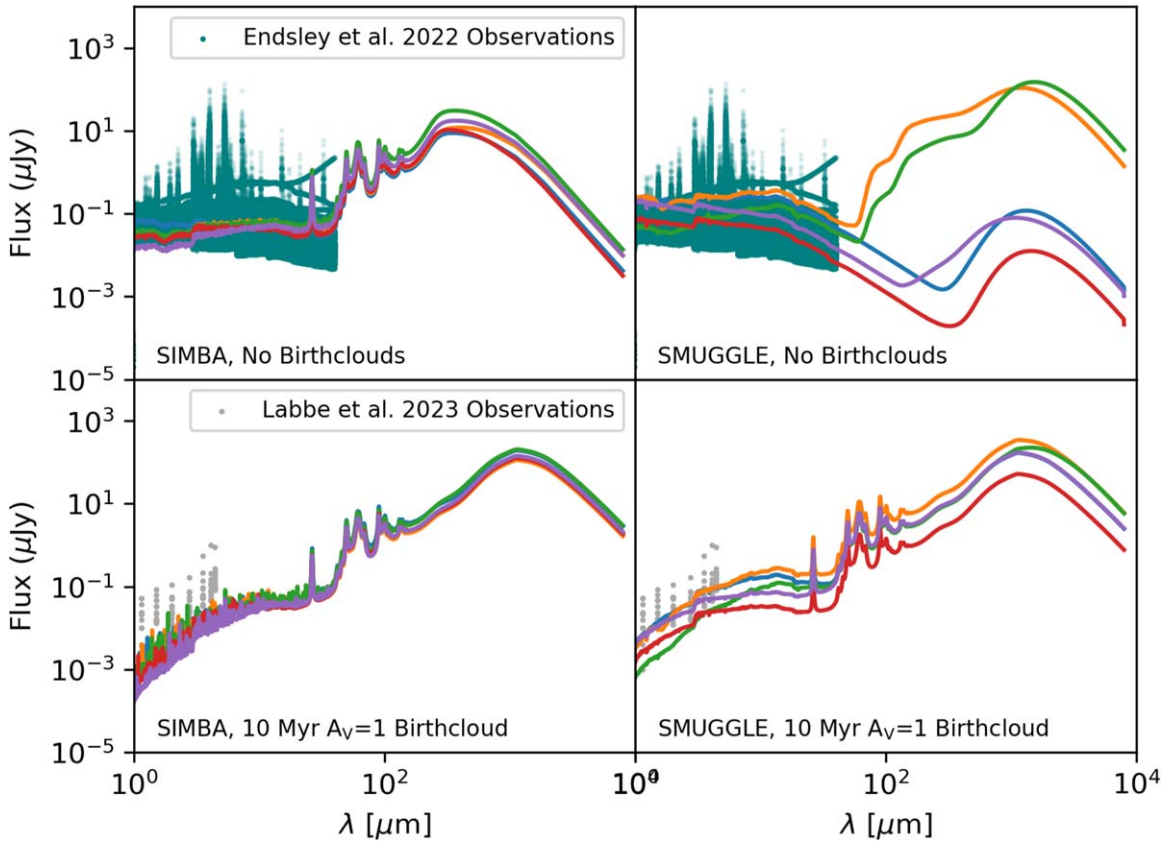

Figure 3. Modeled SEDs for the SIMBA (left) and SMUGGLE (right) models at $z \sim 7.5$. The top row shows the results from POWDERDAY radiative transfer when only the diffuse dust is included, while the bottom row includes Charlot & Fall (2000) birth clouds with an $A_V = 1$ screen in front of all $t < 10$ Myr star particles. The green points show observations from Endsley et al. (2022), while gray points show observations from Labbé et al. (2023). We find that birth clouds dominate the obscuration in the UV/optical.

results. The primary differences in these models as far as this study is concerned are:

1. the stellar feedback model, which impacts the burstiness of the modeled SFHs;
2. the dust model, which impacts the dust content, extinction, and attenuation of the emergent light.

In detail, we employ the SIMBA cosmological simulation, as already run by Davé et al. (2019), as well as a newly run

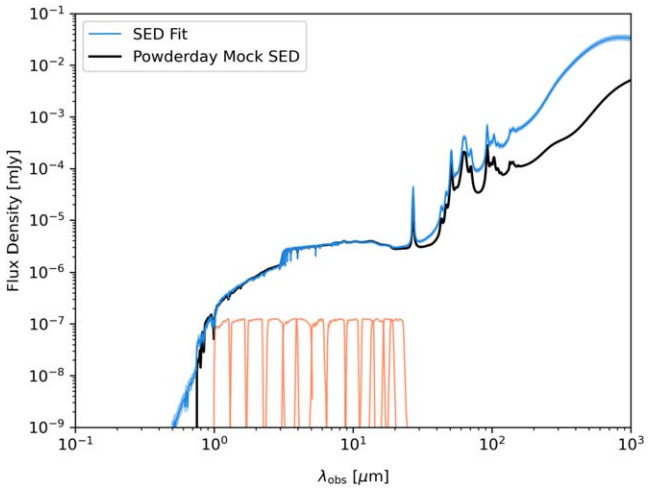

Figure 4. Comparison of SED fit to input SED. The input mock galaxy SED generated by POWDERDAY is in black, while the 16–84th percentile confidence intervals in the fit are denoted by the blue shaded region. The orange lines show the locations of the NIRCAM and MIRI filters for the fit, and the SEDs are redshifted to $z \approx 7$.

simulation employing the SMUGGLE explicit stellar feedback model within the AREPO code base. We briefly describe these models in detail in turn below.

The SIMBA simulation is based on the GIZMO cosmological gravity plus hydrodynamic solver (Hopkins 2015), and evolves dark matter and gas elements together, including gravity and pressure forces. Gas cools radiatively using the GRACKLE library (Smith et al. 2017), including both metal line cooling and nonequilibrium evolution of primordial elements. Stars form in molecular H_2 gas following the Krumholz et al. (2009) subresolution prescription for determining the H I and H_2 content in a gas particle, as well as the Kennicutt (1998) prescription for the star formation rate. Here, a star formation efficiency is manually set to $\epsilon_* = 0.02$. The gas itself is artificially pressurized in order to resolve the Jeans mass as described in Davé et al. (2016). The upshot of this is that the SFH for a given galaxy tends to occur more smoothly than in models with an explicit feedback model (and no artificial pressurization of the interstellar medium (ISM); Iyer et al. 2020). Dust is modeled within SIMBA following the algorithms outlined in Li et al. (2019). Specifically, dust is included as a single-sized particle, though it can comprise multiple species (graphites and silicates). Dust is formed in evolved stars (Dwek 1998), can grow via metal accretion (Asano et al. 2013), and can be destroyed via thermal sputtering in hot gas (Tsai & Mathews 1995; McKinnon et al. 2017; Popping et al. 2017), supernova blast waves, and astration in star-forming regions.

In addition to the SIMBA simulation, we have run simulations with the SMUGGLE galaxy formation model enabled in the AREPO code (Springel 2010; Weinberger et al. 2020). We refer the reader to Marinacci et al. (2019) for a full description of this model, and highlight only the key differences from the SIMBA simulation as they pertain to our study. Star formation occurs only in gravitationally bound molecular gas (Hopkins et al. 2013) and follows a volumetric Kennicutt (1998) law, though with an efficiency $\epsilon_* = 1$. This is in contrast to the forced inefficiency of star formation in SIMBA because on long timescales, stellar feedback in the SMUGGLE model self-regulates the star formation rates to result in the relatively low efficiencies observed in molecular clouds (Marinacci et al. 2019). Stellar feedback models include supernovae, radiative feedback, stellar winds, and thermal feedback from H II regions. Like SIMBA, dust is also included in the SMUGGLE model. In contrast, however, dust is modeled to include a spectrum of grain sizes that evolve as the dust grains evolve in the simulation. Beyond the aforementioned dust processes that are included in SIMBA, the dust in SMUGGLE is allowed to grow in size via coagulation (sticking together), as well as to fragment into smaller grains via grain–grain shattering collisional processes. The upshot from this dust modeling is that the local extinction law is explicitly computed in a spatially resolved sense in galaxies (Li et al. 2021), and represents therefore a fundamental difference in the forward modeling of radiative transfer between the SMUGGLE and SIMBA models. We have simulated a box of $25/h$ Mpc side-length with periodic boundary conditions, starting from $z = 99$ with initial conditions generated with MUSIC (Hahn & Abel 2011). We have run the model at the same mass resolution as the SIMBA simulation (2×512^3 particles), though the initial conditions are generated with different random seeds, so the galaxies are not directly mappable from one simulation to another. We allow the simulation to evolve to redshift $z = 6$, and restrict our analysis to this redshift range.

2.3. Dust Radiative Transfer

In order to generate the mock SEDs (that we will then fit using PROSPECTOR), we employ the public POWDERDAY dust radiative transfer package (Narayanan et al. 2021), which employs YT, FSPS, and HYPERION for grid generation, stellar population synthesis, and Monte Carlo radiative transfer respectively (Conroy et al. 2009; Robitaille 2011; Turk et al. 2011). Here, stars that form in the simulation of galaxy formation emit a stellar spectrum based on their ages and metallicities. This spectrum is computed using FSPS (Conroy et al. 2009, 2010; Conroy & Gunn 2010). We assume the MIST stellar isochrones (Choi et al. 2016) and a Kroupa (2002) stellar initial mass function (IMF) (consistent with both sets of hydrodynamic simulations). We note that the choices of these parameters can subtly impact our results. For example, different isochrone models can change the assumed lifetimes of massive stars, which will impact the degree of outshining that we model here.

The light from these stars[16] is emitted in an isotropic manner, and can be absorbed, scattered, and re-emitted by dust in the individual cells in the galaxy. For the SIMBA simulations, which are particle-based, the dust information is smoothed from the particles onto an adaptive mesh with an octree memory structure, and the radiative transfer occurs on this grid. For SIMBA we assume Weingartner & Draine (2001) dust extinction laws locally. For SMUGGLE, we perform the radiative transfer on a Voronoi mesh built around the dust particles simulated with the active dust model, and compute the extinction laws explicitly in each cell following Narayanan et al. (2023). Here, we assume extinction efficiencies from Draine & Lee (1984) and Laor & Draine (1993) for silicates and carbonaceous grains respectively.

[16] We note that H II regions around massive stars could generate nebular emission lines in the UV/optical, which can possibly impact broadband photometry (e.g., Stark et al. 2013; Giménez-Arteaga et al. 2023). Indeed, some work has already been done to include nebular lines in POWDERDAY (e.g., Garg et al. 2022), and this emission (once computed) is simply tacked onto the stellar SEDs for the dust radiative transfer phase. This said, we aim to isolate the uncertainties incurred by the SED fits in our simulations to the SFHs, and therefore do not include this additional physics in either the forward modeling or the SED fitting. Future work will investigate the role of nebular emission in contaminating broadband fluxes in galaxies.

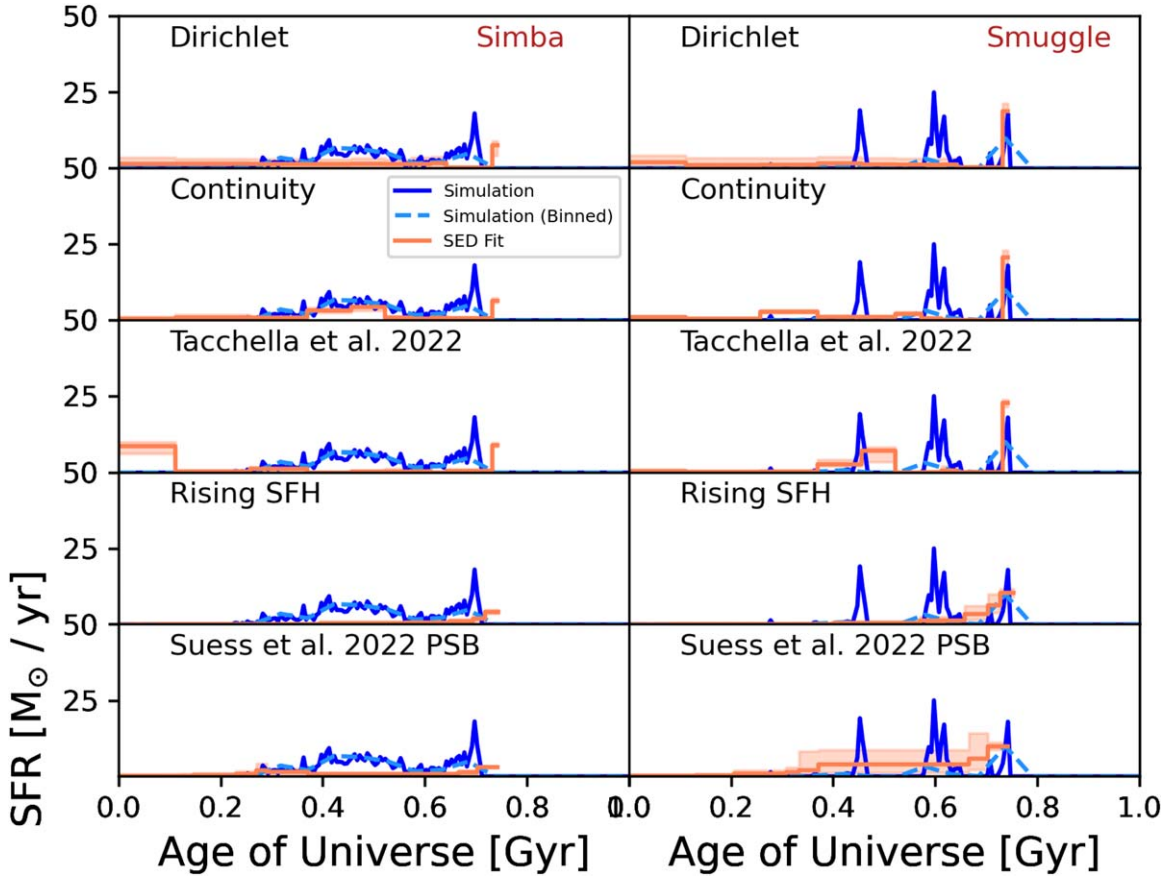

Figure 5. SFHs for arbitrarily chosen galaxies from the SIMBA simulation (left) and SMUGGLE simulation (right), with the best-fit derived SFHs from SED modeling overlaid (orange). The simulated SFH binned at the same time resolution as the SED fits is shown as a lighter, dashed blue line. Owing to outshining by recently formed stellar populations, early stellar mass buildup can be missed by SED modeling. This will have a significant impact on the derived stellar masses (see Figure 6).

Beyond attenuation by the diffuse dust in the galaxy (which is explicitly modeled in both SIMBA and SMUGGLE), POWDERDAY includes the possibility of obscuration by subresolution "birth clouds" following the Charlot & Fall (2000) formalism as built into FSPS. Here, the attenuation only occurs for star particles below a threshold age (we set this to $t = 10$ Myr when included), and it has a user-defined normalization to the attenuation curve, which we set as $A_V = 1$. We discuss this in further detail in Section 3.2.

3. The Physical and Luminous Properties of $z > 7$ Galaxies

3.1. Stellar Masses and SFHs

We begin our analysis by describing the physical and luminous properties of our model galaxies. In Figure 1, we plot a distribution of the stellar masses at $z = 7$ of the 20 most massive galaxies in the SIMBA and AREPO simulations. In a $(25\ \mathrm{Mpc}/h)^3$ volume, the most massive galaxies at $z \approx 7.5$ have $M_* \sim 10^8$–$10^9\ M_\odot$. These stellar masses are, by and large, built up via a series of individual star formation episodes, though the importance of these bursts to the total buildup of stellar mass (and, in general, the shape of the SFH) is dependent on the assumed stellar feedback model (e.g., Sparre et al. 2017; Iyer et al. 2020). In Figure 2, we show the SFHs for five arbitrarily chosen galaxies from each simulation. The SFH is constructed from the $z \approx 7$ snapshot using the $z = 7$ stellar ages, correcting for mass loss processes.

The SIMBA model with a manifestly pressurized ISM model broadly has a smoother rising SFH, with punctuated bursts superposed. In comparison, the SMUGGLE stellar feedback model is dominated by individual bursts at these high redshifts, owing to the explicit nature of the feedback model. The two models bracket the smoother SFHs typically seen in simulations with a pressurized ISM (e.g., EAGLE, ILLUSTRIS, and SIMBA), and the burstier SFHs seen in explicit feedback models (e.g., FIRE and SMUGGLE). It is the ability to reconstruct these SFHs with reasonably high fidelity (or lack thereof) that will prove essential for the SED fitting software to accurately derive the stellar masses of galaxies in this epoch.

3.2. Model SEDs

In the top row of Figure 3, we show the model SEDs for the same arbitrarily chosen galaxies as in Figure 2 at $z = 7.5$. As a reminder (see Section 2.2), the SIMBA model actively models the dust content of the galaxies on-the-fly in the simulation but does not model the grain size distribution. As a result, the interstellar extinction curves are assumed to be those of Weingartner & Draine (2001). In contrast, the SMUGGLE model includes a grain size distribution as well, and therefore the radiative transfer used to generate the mock SEDs in Figure 2 includes the spatially varying dust extinction curves. The SIMBA model uses a Milky Way template for polycyclic aromatic hydrocarbon emission (scaled for the local energy deposited), while the SMUGGLE model uses the Draine et al. (2021) model, based on the local grain populations

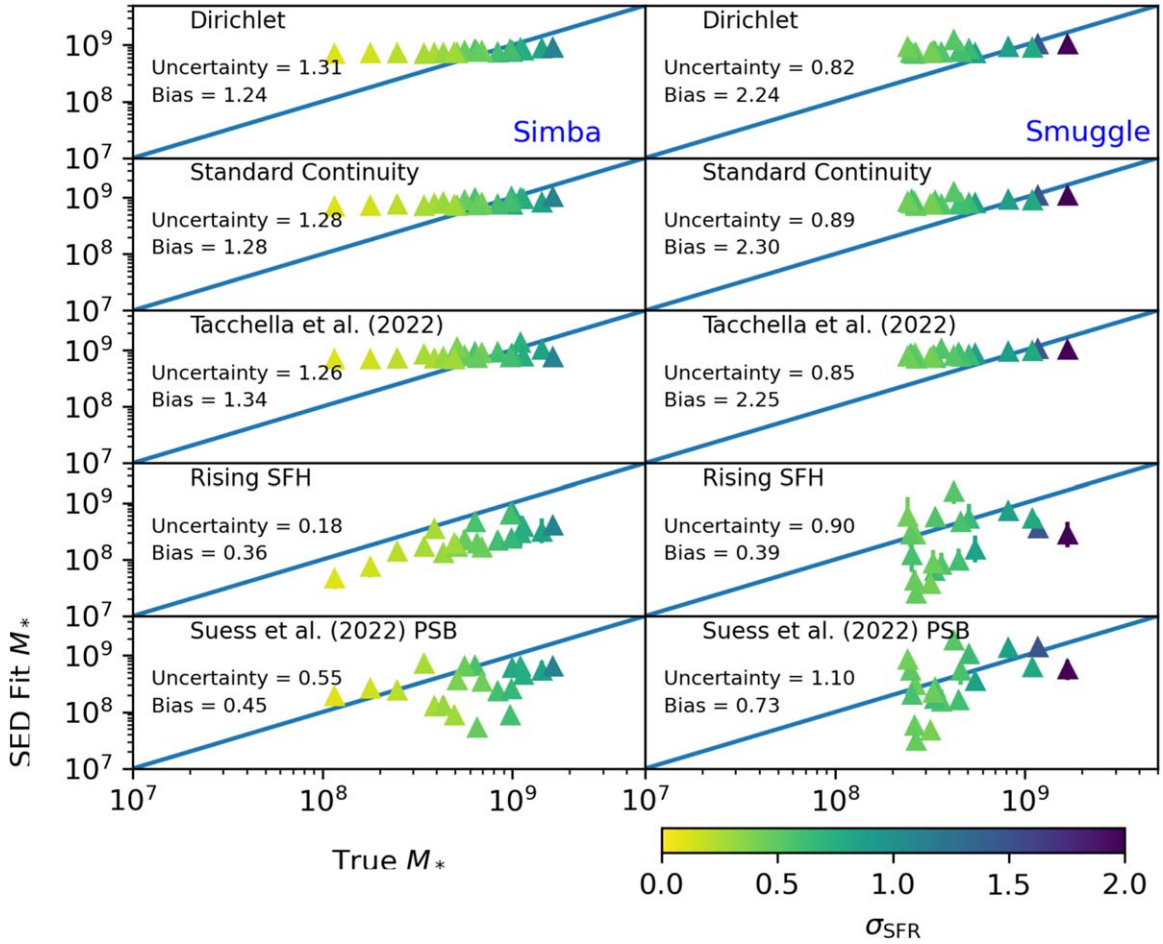

Figure 6. Comparison of the best-fit-derived M_* from SED fitting to the true M_* for the SIMBA model (left) and the SMUGGLE model (right). The result of poorly fit SFHs (Figure 5) is uncertainties of up to an order of magnitude in the derived stellar masses of high-z galaxies with systematic trends in over- or underestimating M_* depending on the nature of the exact prior used. The color coding shows σ_{SFR}, which is the standard deviation in the star formation rates over the lifetime of the galaxy and is a measure of the 'burstiness' of the system. The uncertainty is measured as the standard deviation of M_*(fit)/M_*(true), while the bias is measured as the median of M_*(fit)/M_*(true). Generally, the SIMBA simulation exhibits less burstiness (see Figure 2). The uncertainties and biases vary dramatically, though the priors that favor rising SFHs (e.g., Wang et al. 2023), as well as those that allow for more dramatic SFH variations (e.g., Suess et al. 2022), tend to perform the best.

(Narayanan et al. 2023), which results in fairly different mid-IR emission features. Therefore, as in modeling the SFHs, the two dust models that we include here bracket a reasonable range of modeled dust extinction and obscuration. In the bottom row of Figure 3, we show the same SEDs, but this time include Charlot & Fall (2000) "birth clouds" around young stars. These birth clouds are included in a subresolution fashion such that any star particle with age $t_{age} < 10^7$ yr experiences an extra attenuation of $A_V = 1$. We show observational comparisons from the Endsley et al. (2022)[17] and Labbé et al. (2023) surveys in the top and bottom, respectively (these are split in the top and bottom for clarity).

Two immediate points are clear from Figure 3. First, the model SEDs that we present here provide a reasonable match to observations,[18] including SEDs that have relatively blue and relatively red optical spectra. This allows us to proceed in our analysis with reasonable confidence in our methods. Second, the observations exhibit a wide range of rest-frame optical colors, with (as a general statement) the sources of Labbé et al. (2023) being redder than the galaxies of Endsley et al. (2022). When comparing against our models, it is immediately evident that the majority of reddening in $z > 7$ galaxies is due to local obscuration at the sites of very young stars; diffuse dust in the ISM is insufficient to provide the required reddening to match the observed NIRCAM photometry for the reddest sources. This latter point is a net win for galaxy SED fitting: many modern SED fitting codes have the ability to include such clouds in their backward modeling. This reduces the uncertainties incurred by the diverse shapes of diffuse ISM attenuation curves (Narayanan et al. 2018; Trayford et al. 2020; Lower et al. 2022).

4. Recovering the Stellar Masses of Redshift >7 Galaxies via SED Fitting

Having established the nature of SFHs in the early Universe (at least within the context of two reasonably plausible galaxy formation models), as well as the forward modeled SEDs from these galaxies, we now ask how accurately we can recover the stellar masses of these model galaxies by fitting the mock SEDs. We fit these SEDs with PROSPECTOR (Johnson et al. 2019), assuming full JWST NIRCAM and MIRI coverage of

[17] Note that the data presented here, formally, are the BEAGLE SED fits to the data.
[18] Noting, of course, the lack of emission lines in either our forward or backward modeling. We reiterate that this is intentional so as to isolate the uncertainties modeled here to SFH modeling.

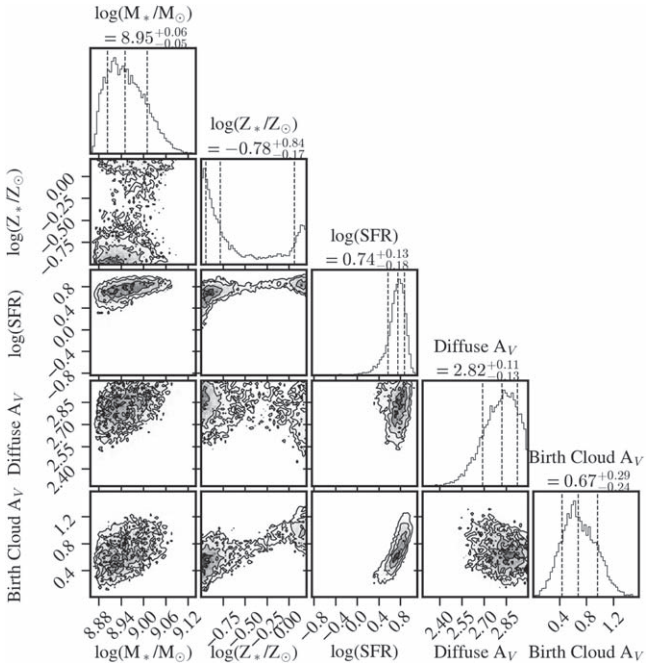

Figure 7. Example PROSPECTOR model parameter posteriors for an arbitrarily chosen SIMBA galaxy fit with the Dirichlet prior SFH model. The true physical quantities are $\log(M_*/M_\odot) = 9.2$, $\log(\mathrm{SFR}/M_\odot\ \mathrm{yr}^{-1}) = 0.85$, and $\log(Z/Z_\odot) = -1.8$. The stellar mass is moderately degenerate with the dust attenuation parameters while the SFR is highly degenerate with the dust component of the birth cloud. The stellar metallicity posterior is bimodal, so is not well constrained by the data.

the rest-frame UV–near-IR SEDs (noting that this is assuming a relatively optimistic wavelength coverage).

By using PROSPECTOR for the backward modeling, we are able to minimize the uncertainty incurred by many of the choices of stellar population parameters because fundamentally PROSPECTOR and POWDERDAY both use FSPS under the hood to model stellar populations. We therefore assume the *exact same* model IMF, spectral libraries, and stellar isochrone models in order to obviate these potential uncertainties in our SED modeling. We additionally fix the redshift to the true redshift of the galaxy to avoid uncertainties in the redshift fit. We assume a uniform (and arbitrarily chosen) signal-to-noise ratio of 10 across all bands. We allow the birth cloud model in the SED fits to be flexible.

We assume the nonparametric form for modeling SFH where the SFHs are constrained with a set of three model priors.

1. The *Dirichlet prior* (Betancourt & Girolami 2013) is parameterized by concentration index α, which sets the preference for all stellar mass to be formed in a single bin versus a smoother distribution of stellar mass formed over the modeled time period. We have run tests for the range $\alpha = [0.3, 1.0]$ and found minimal impacts on our results.
2. The *standard continuity prior* fits for $\Delta\log(\mathrm{SFR})$ between SFH time bins, thus weighting against dramatic variations in the SFH between adjacent time bins. This weighting is parameterized by a Student's t-distribution (Leja et al. 2019a). This is given by $x = \log(\mathrm{SFR}_n/\mathrm{SFR}_{n+1})$, where

$$\mathrm{PDF}(x, \nu, \sigma) = \frac{\Gamma\left(\frac{\nu+1}{2}\right)}{\sqrt{\nu\pi}\,\Gamma\left(\frac{\nu}{2}\right)}\left(1 + \frac{(x/\sigma)^2}{\nu}\right)^{-(\nu+1)/2} \quad (1)$$

Here, Γ is the Gamma function, σ controls the width of the distribution, and ν controls the tail of the distribution function. Following Leja et al. (2019a), we set $\nu = 2$ and $\sigma = 3$.
3. The *bursty continuity prior*, developed by Tacchella et al. (2022), adjusts the parameters in the Student's t-distribution to $\sigma = 1$ and $\nu = 2$, resulting in a burstier SFH.
4. The *rising SFH prior* was developed by Wang et al. (2023) to preferentially favor rising SFHs.
5. The *post-starburst prior* was developed by Suess et al. (2022) for post-starburst galaxies that have sharp changes in their recent SFHs.

These SFH priors are not meant to be comprehensive, but rather to span a range of reasonable priors commonly used in the literature, and to demonstrate the potential impact of these priors on the derivation of galaxy stellar masses in the early Universe.

In Figure 4, we show an example fit for one of our model SEDs, with the observational filters overlaid (we zoom in to the NIRCAM/MIRI wavelengths). The blue shaded region denotes the 16%–84% percentile confidence intervals in the posterior, while the black line shows the input POWDERDAY mock SED. The fit was performed at $z \approx 7$. The quality of fit presented in Figure 4 is comparable to all of the fits performed for this study.

In Figure 5, we show the model SFH for an arbitrarily chosen galaxy from both the SIMBA and SMUGGLE simulations with the best-fit SFH as derived from the PROSPECTOR fits with each of these priors imposed (we show this same plot for all modeled galaxies in the Appendix). In the left column we show the results for an arbitrarily chosen galaxy from the SIMBA simulation, while in the right we show the results from the SMUGGLE model. The orange lines show the median best-fit SFH from PROSPECTOR, while the shaded region shows the interquartile dispersion. The simulated SFH is shown in solid blue, and in dashed lighter blue we bin the simulated SFH at the same time resolution. As is clear, none of the imposed SFH priors adequately reproduces the SFH of the early Universe in either galaxy formation model, though the models that allow for the most dramatic star SFH variations perform the best.

In detail, the Dirichlet prior constrains the fraction of mass formed in each time bin (in the model SFH) such that the fractional specific SFR in each time bin follows the Dirichlet distribution. While some variation in the fractional contribution to the total stellar mass from a given SFH bin is allowed, such variations do not tend to be dramatic with the Dirichlet prior (Leja et al. 2017). As a result, the early SFH for each model is a relatively low-level, constant SFR, with the dominant changes happening in the latest time bins, where the majority of the light contributes to the SED. The continuity prior is similar to the Dirichlet one, though as discussed, it favors less dramatic variations in the SFH. The default continuity prior was tuned by Leja et al. (2019a) to the Illustris-TNG SFHs, which are relatively smooth (owing to the effective equation of state pressurizing the interstellar medium). As a result, the default continuity prior (as we employ here) will therefore demonstrate even less power on short timescales (Leja et al. 2019a; Lower et al. 2020). The Tacchella et al. (2022) prior modifies this continuity prior to allow for a burstier SFH, though we still find that these modifications are insufficient to result in the level of burstiness seen in the SIMBA and SMUGGLE simulations. Because of this, the low-level, nearly constant SFH at early times dominates the stellar mass buildup with the Dirichlet, continuity, and Tacchella et al. (2022) modifications to the

continuity priors, giving somewhat similar derived stellar masses for all model galaxies.

The rising SFH, developed by Wang et al. (2023), favors rising SFHs. Generally, the SFHs for both the SIMBA and SMUGGLE models rise with time, with the burstiness of the SFH as the main variant between the two. As a result, the rising SFH prior of Wang et al. (2023) performs quite well on the SIMBA galaxy formation model, which has relatively minor bursts, and moderately well on the burstier SMUGGLE SFH. Finally, the Suess et al. (2022) SFH prior is a two-component prior designed to fit the SFH of post-starburst galaxies: in particular, it allows for sharp changes in the recent SFH. As a result, while the Suess et al. (2022) prior is designed for post-starburst galaxies, it performs reasonably well for our model high-z galaxies owing to their highly time-variable SFHs.

We show the impact of these SED fits on the derived stellar masses in Figure 6, where we compare the SED-fit M_* to the true M_* for each galaxy, with panels ordered akin to Figure 5. We color-code the galaxies with a measure of their SFH "burstiness," here parameterized as the standard deviation of the SFR over the history of the Universe. We additionally provide summary statistics for each model via the uncertainty (quantified as the standard deviation of $M_*(\mathrm{fit})/M_*(\mathrm{true})$) and the bias (quantified as the median of the same ratio). Smaller uncertainties, and biases that are closer to unity demonstrate higher accuracy in the derived stellar masses.

Generally, no model performs particularly well, with uncertainties including both overestimates and underestimates. The lack of early star formation in the SED fits owes to "outshining": the most recent burst of star formation dominates the SED, and therefore has a significantly outsized impact on the resulting fit. The SFH priors that allow for rising SFHs, as well as those that allow for the most dramatic variations in the SFH, quantitatively perform the best (bottom two rows of Figure 6), though neither fully capture the very recent variability in star formation.

Whether an SED fit overpredicts or underpredicts the true stellar mass depends in large part on the amount of early star formation that the SED fit predicts. In Figure 7, we show the corner plot for an arbitrarily chosen SIMBA galaxy using the Dirichlet prior. There are significant uncertainties in the derived physical properties as well as covariances between them, specifically between stellar mass and SFR and the dust attenuation parameters. These degenerate solutions make inferring the true galaxy properties difficult when the available data do not have enough constraining power.

We caution that these results are particular to the bands employed here (NIRCAM+MIRI), as well as the particulars of the SFHs modeled, and are therefore intended to demonstrate the range of uncertainty rather than the specific direction of uncertainty in M_* estimates at high z. The takeaway from this analysis is not that a particular SFH prior tends to underpredict or overpredict stellar masses at high redshift, but rather a demonstration of the relative level of uncertainty in fitting the SEDs of galaxies whose stellar masses are dominated by early star formation that is being outshined by current star formation.

5. Discussion

5.1. General Discussion

We have, thus far, seen that when observing galaxies at high redshift (here, we model $z \gtrsim 7$), SED fitting techniques have difficulty in correctly inferring the stellar masses of galaxies owing to the substantial contribution of stellar mass buildup by individual star formation episodes at earlier times. This is true for a range of SFHs, ranging from the smoother SFHs seen in traditional cosmological simulations to more bursty SFHs in explicit feedback models. The fundamental issue is that current star formation at the time of detection is able to outshine the prior stellar mass buildup, making it difficult for SED fitting software to infer its presence. This situation will be most extreme for very bursty systems, though at least within the context of the range of models explored here it appears to be a generic problem. Whether SFHs at high z are bursty in the early Universe remains an open question, though recent observations and models appear to suggest at least some level of burstiness (e.g., Dressler et al. 2023; Endsley et al. 2023; Shen et al. 2023).

As these systems evolve to lower redshift, it is expected that traditional SED fitting techniques will perform substantially better as the ratio of flux from current star formation to that from the integrated stellar mass buildup decreases. Indeed, this was demonstrated explicitly by Lower et al. (2020), who performed experiments similar to those presented in this paper for $z = 0$ model galaxies in the SIMBA simulation, and found that SED fitting with nonparametric SFH models could accurately determine galaxy stellar masses.

This said, we note some caution when interpreting the results presented here. The simulations here encompass two different models for stellar feedback that result in varied SFHs, for galaxies drawn from a relatively small box ($25/h$ Mpc on a side). While these models span a diverse range of SFHs for galaxies of similar mass, they are not necessarily comprehensive. It is possible that some model forms of SFH (i.e., where most of the mass is formed at the time of observation) could result in highly accurate derivations of the stellar mass. Similarly, the modest size of our cosmological boxes excludes the most massive and rare systems. These results should not be taken to mean that a particular SFH prior will always overpredict or always underpredict stellar masses: the exact relationship between the modeled stellar masses of galaxies and true ones depend on a wide range of choices in SED modeling (e.g., Conroy 2013; Lower et al. 2020; Gilda et al. 2021). Instead, these results are simply intended to reflect the uncertainty associated with SED modeling of galaxies in the early Universe.

5.2. Relationship to Other Studies

While we have explicitly demonstrated the issue of deriving stellar masses in high-z galaxies via direct numerical simulation, this issue has been hypothesized in the observational literature in a wide range of contexts. For example, Tacchella et al. (2022) studied the stellar populations of 11 galaxies from $9 < z < 11$ and found that the inferred stellar ages were significantly impacted by the assumed SFH prior; they noted that multiple priors were able to fit the data equivalently. Similarly, Topping et al. (2022) modeled the stellar masses of UV-selected galaxies at $z \sim 7$–8 and found that the derived stellar masses can be uncertain by up to an order of magnitude owing to the outshining of older stellar populations by a current burst. Whitler et al. (2023) modeled the stellar ages of UV-bright $z \sim 7$ galaxies and found a potential tension between the relatively young inferred stellar ages of their sample and the detection rate of higher-redshift sources by JWST. This tension

can be alleviated if the $z \sim 7$ galaxies have older stellar components formed in earlier bursts, as in the simulations presented here. Giménez-Arteaga et al. (2023) fit spatially resolved measurements of $5 < z < 9$ galaxies in the JWST SMACS 0723 field with BAGPIPES (Carnall et al. 2018) and found evidence for a bursty SFH as well as potential for an older stellar population (outshined by current star formation). When taking this outshining into account, Giménez-Arteaga et al. (2023) found inferred stellar masses reduced by 0.5–1 dex. Finally, Iyer et al. (2019) note, in their development of the dense-basis methodology for nonparametric SFH reconstruction from observed galaxy SEDs, that the ability to model older stellar populations is prior-dominated rather than likelihood-dominated and that sharp variations in the SFH may be difficult to infer.

In addition to studying the impact of outshining on the inference of the stellar mass of high-z galaxies, we have additionally analyzed the impact of SFH priors on the derived masses. The inference of SFHs has been demonstrated by a number of authors to be strongly dependent on the assumed priors for the SFH. For example, Leja et al. (2019a) have derived stellar masses 0.1–0.3 dex larger using nonparameric SFHs as opposed to traditional parametric models in the 3D-HST galaxy catalog. Similarly, studying galaxies at $z > 7$, Tacchella et al. (2022) and Whitler et al. (2023) found inferred stellar ages and masses to be highly sensitive to the form of the assumed SFH in the SED fitting. Finally, Suess et al. (2022) showed that the assumed SFH priors can substantially impact the inferred ages of post-starburst galaxies via synthetic stellar population modeling.

5.3. Possible Ways Forward

The primary outcome of this paper is to demonstrate the uncertainty of the measurement of high-z stellar masses. We advocate for investment by the community in the development of methods to reduce the bias and uncertainty in these measurements.

One possibility is through the development of new SFH priors in SED fitting codes. Already we have seen in Figure 6 that priors that allow rapid transitions in SFH perform reasonably well. In a similar vein, including information from spectral line features that trace star formation over different timescales may help to quantify the burstiness and to inform the modeling of the SFH (e.g., Iyer et al. 2022).

As an alternative to traditional SED fitting techniques, machine learning methods may hold promise. Gilda et al. (2021) demonstrated the efficacy of using mock SEDs from large cosmological simulations as a training set for machine learning-based SED fitting software. Gilda et al. (2021) demonstrated that in some circumstances these techniques can far outperform traditional SED fitting.

6. Summary and Outlook

In this paper, we have employed cosmological simulations of galaxy evolution in order to investigate the ability of modern SED fitting techniques to recover the stellar masses of high-redshift galaxies. Owing to the relatively young ages of $z \gtrsim 7$ galaxies, early bursts of star formation constitute a significant fraction of the formed mass at the time of SED modeling. As a result, if the stellar light from this early star formation (see Figure 5) is outshined by late-time star formation at the time of detection, then the recovered stellar masses can be incorrect by nearly an order of magnitude (Figure 6). The impact of these uncertainties will decrease at lower redshifts, as the ratio of the light emitted from star formation at the time of detection to the light from the underlying stellar mass decreases. As JWST pushes the frontier of high-redshift science to increasingly early times, we encourage the development of new techniques in order to accurately derive the physical properties of these first galaxies.

Acknowledgments

The authors thank the anonymous referee for a careful and timely review of this paper. D.N. expresses gratitude to Adriano Fontana, Paola Santini, and the organizors of "The Growth of Galaxies in the Early Universe—VIII," where the idea for this paper was born out of discussions at the Bad Moos. D.N. additionally thanks the Aspen Center for Physics, which is supported by National Science Foundation grant PHY-1607611, which is where the original framework for the POWDERDAY code base was developed. D.N. thanks Mike Boylan-Kolchin, Chris Hayward, Chia-Yu Hu, Pavel Kroupa, Justin Spilker, Wren Suess, and Sandro Tacchella for helpful conversations, as well as Ryan Endsley for providing data from Endsley et al. (2022) for comparison against our models. D.N. and P.T. were supported by NASA ATP grant 80NSSC22K0716. W.C. is supported by the STFC AGP Grant ST/V000594/1 and the Atracción de Talento Contract no. 2020-T1/TIC-19882 granted by the Comunidad de Madrid in Spain. He also thanks the Ministerio de Ciencia e Innovación (Spain) for financial support under Project grant PID2021-122603NB-C21 and ERC: HORIZON-TMA-MSCA-SE for supporting the LACEGAL-III project with grant number 101086388. The Cosmic Dawn Center is funded by the Danish National Research Foundation (DNRF) under grant #140.

Appendix

In Figures 8–27 we show the model SFH for all of our simulated galaxies, as well as the PROSPECTOR SED fits (for every modeled SFH prior) for each galaxy. The galaxies are ordered by mass (i.e., for an individual plot, the SIMBA galaxy and SMUGGLE galaxy each represent the Nth most massive galaxy in the cosmological volume.

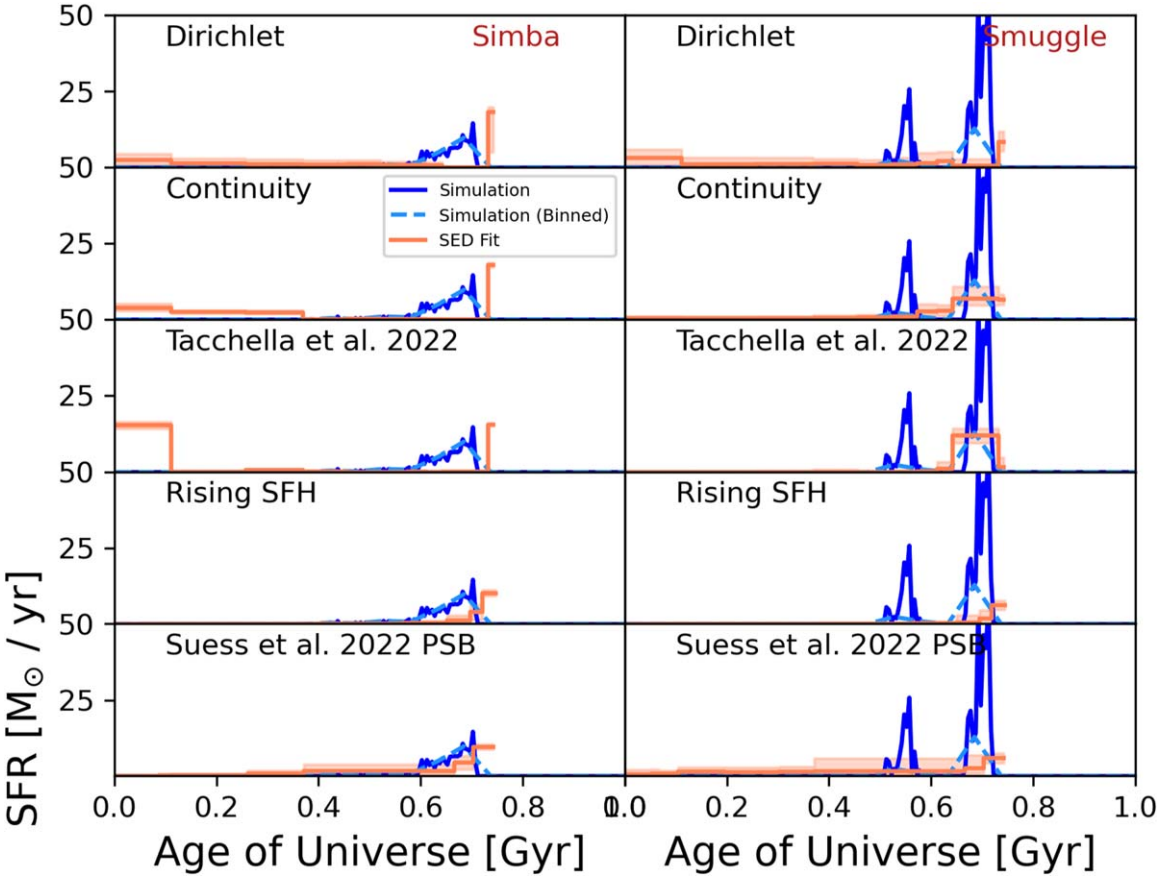

Figure 8. SFHs for the most massive galaxy in the SIMBA (left) and SMUGGLE (right) simulations.

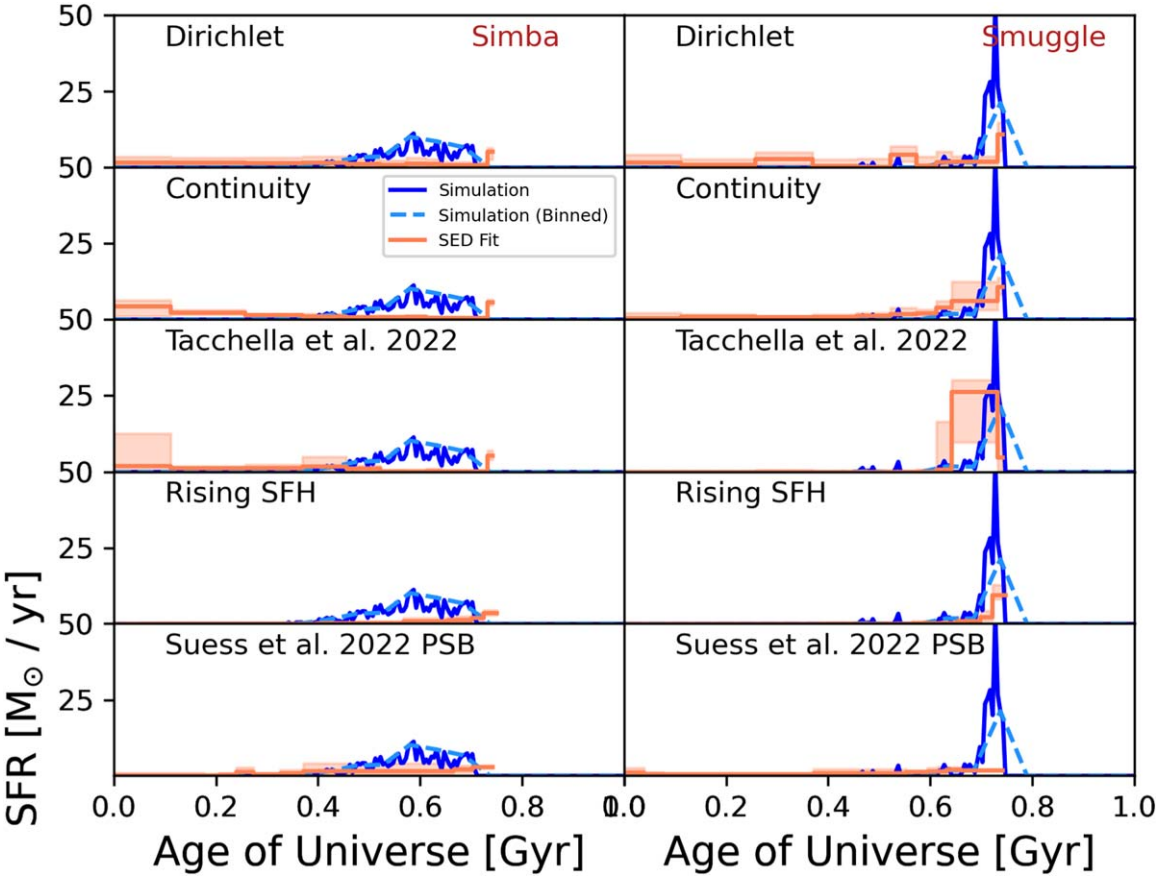

Figure 9. SFHs for the second most massive galaxy in the SIMBA (left) and SMUGGLE (right) simulations.

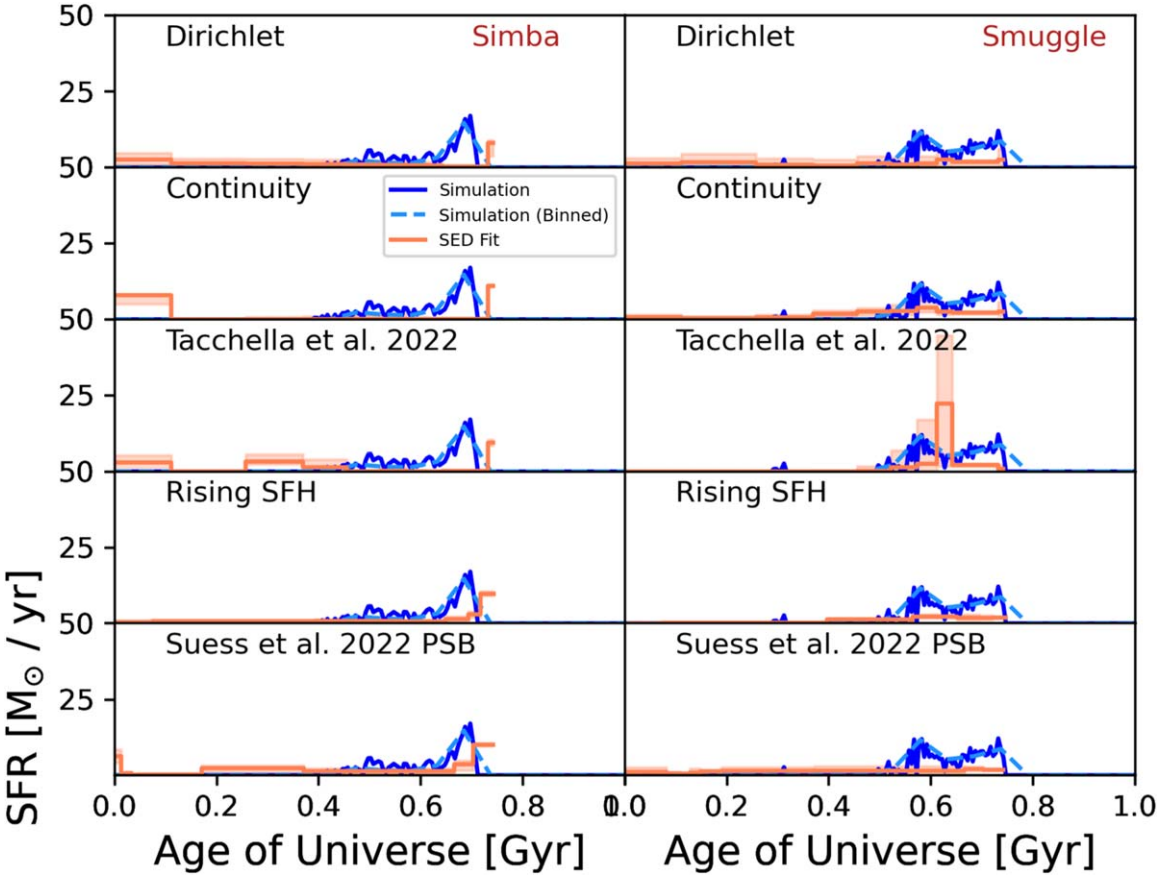

Figure 10. SFHs for the third most massive galaxy in the SIMBA (left) and SMUGGLE (right) simulations.

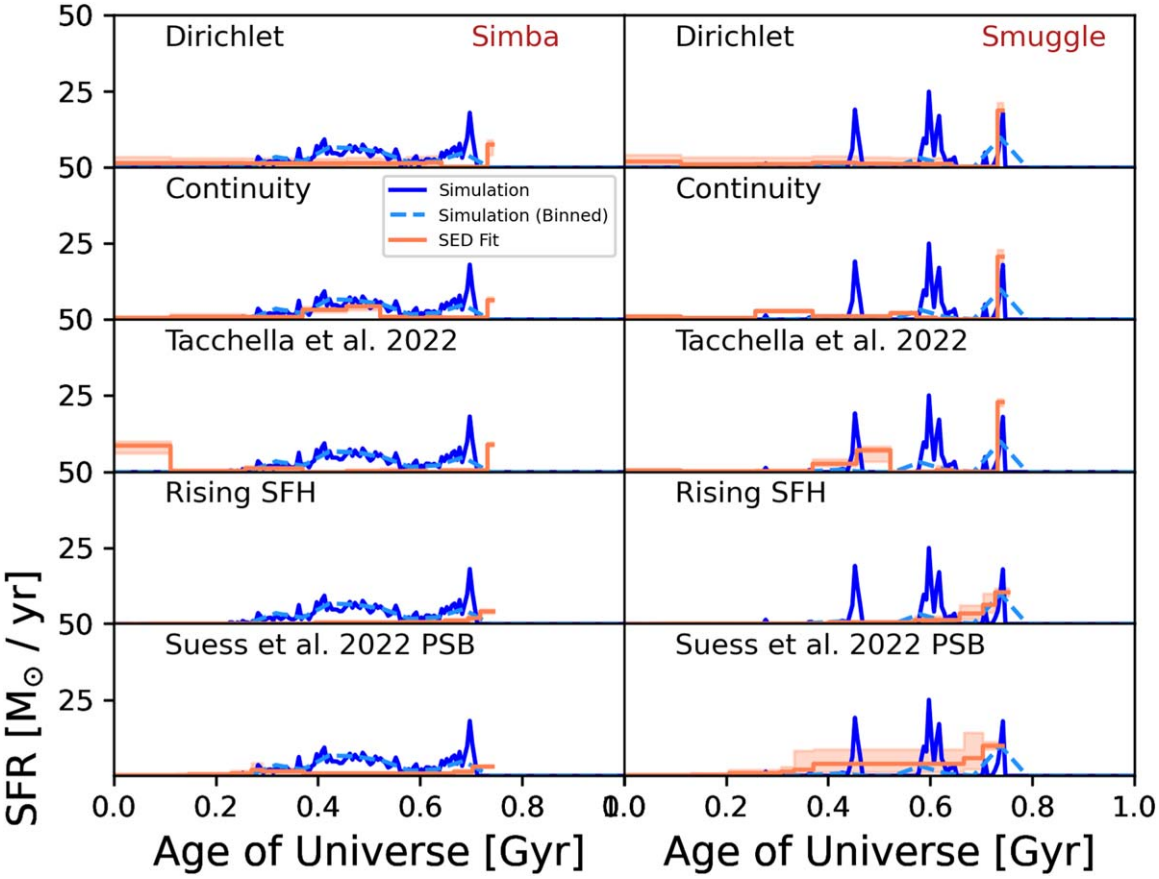

Figure 11. SFHs for the fourth most massive galaxy in the SIMBA (left) and SMUGGLE (right) simulations.

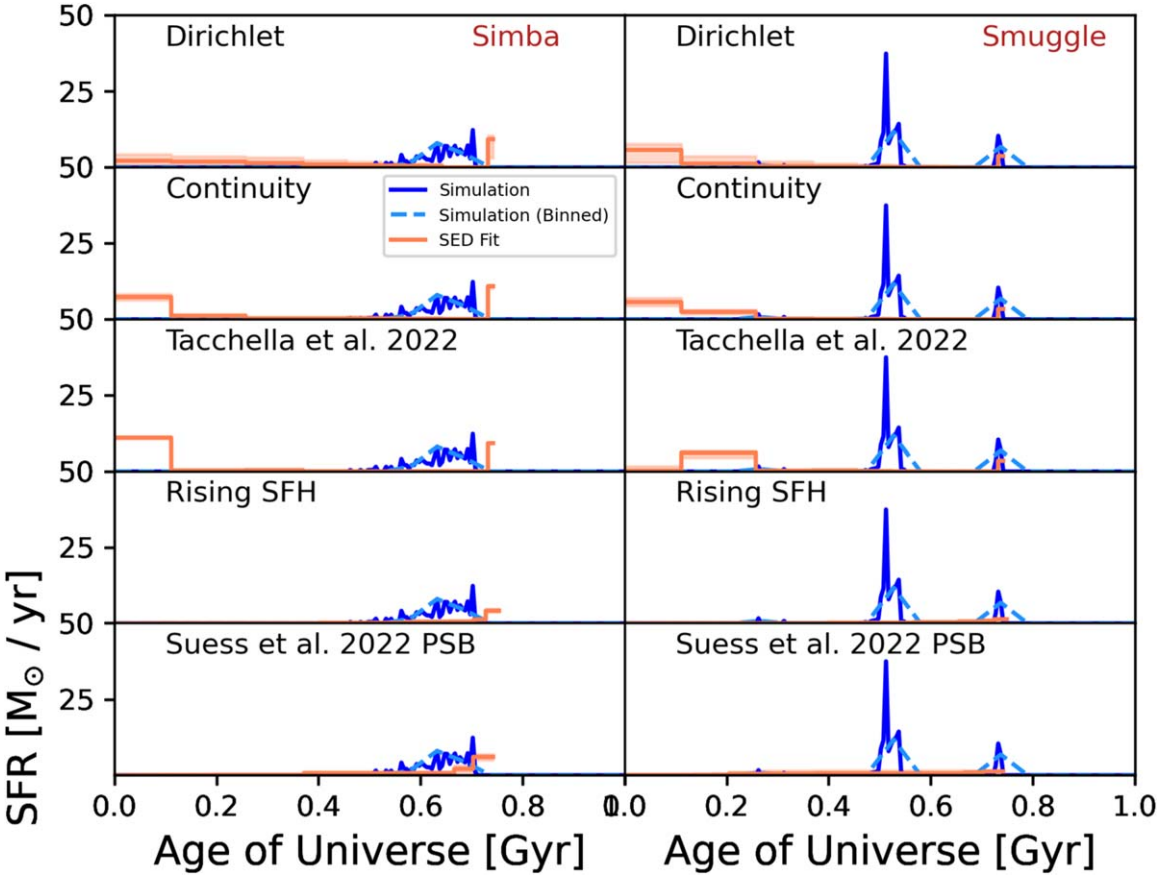

Figure 12. SFHs for the fifth most massive galaxy in the SIMBA (left) and SMUGGLE (right) simulations.

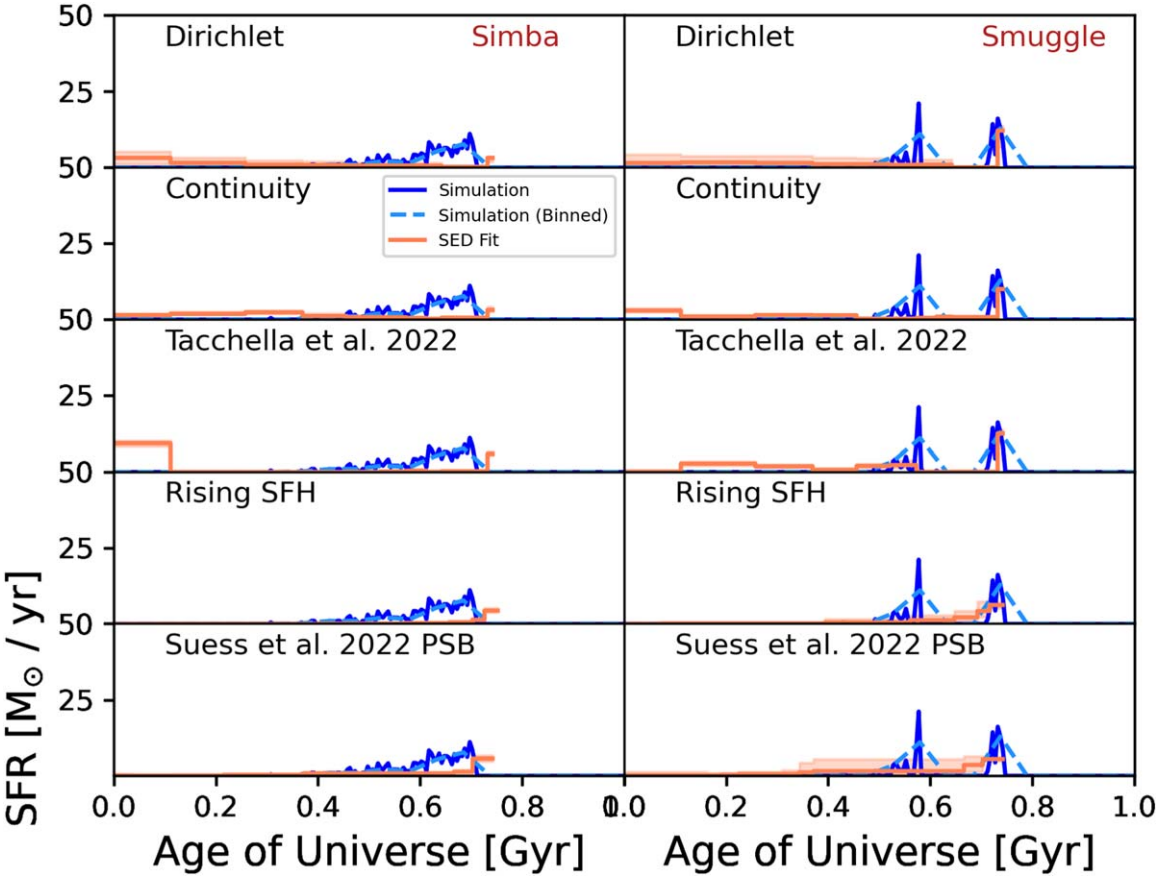

Figure 13. SFHs for the sixth most massive galaxy in the SIMBA (left) and SMUGGLE (right) simulations.

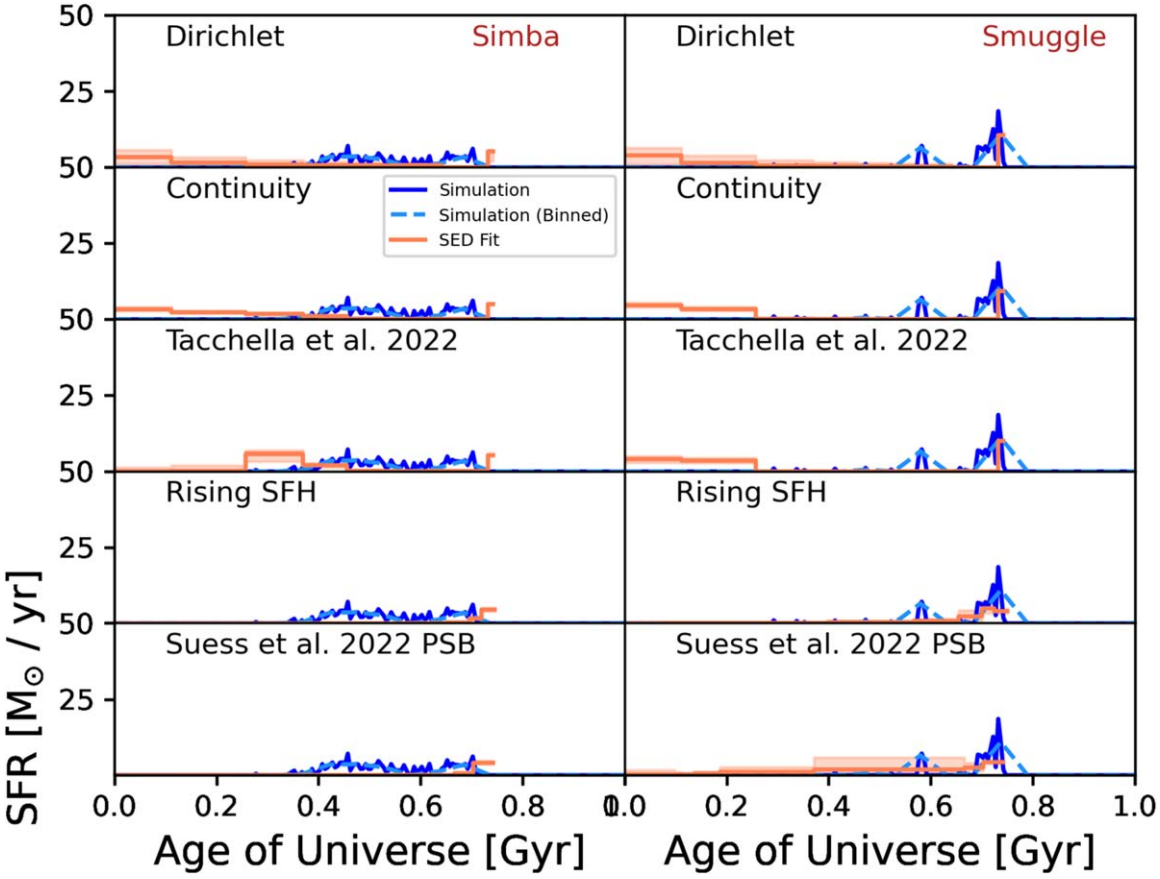

Figure 14. SFHs for the seventh most massive galaxy in the SIMBA (left) and SMUGGLE (right) simulations.

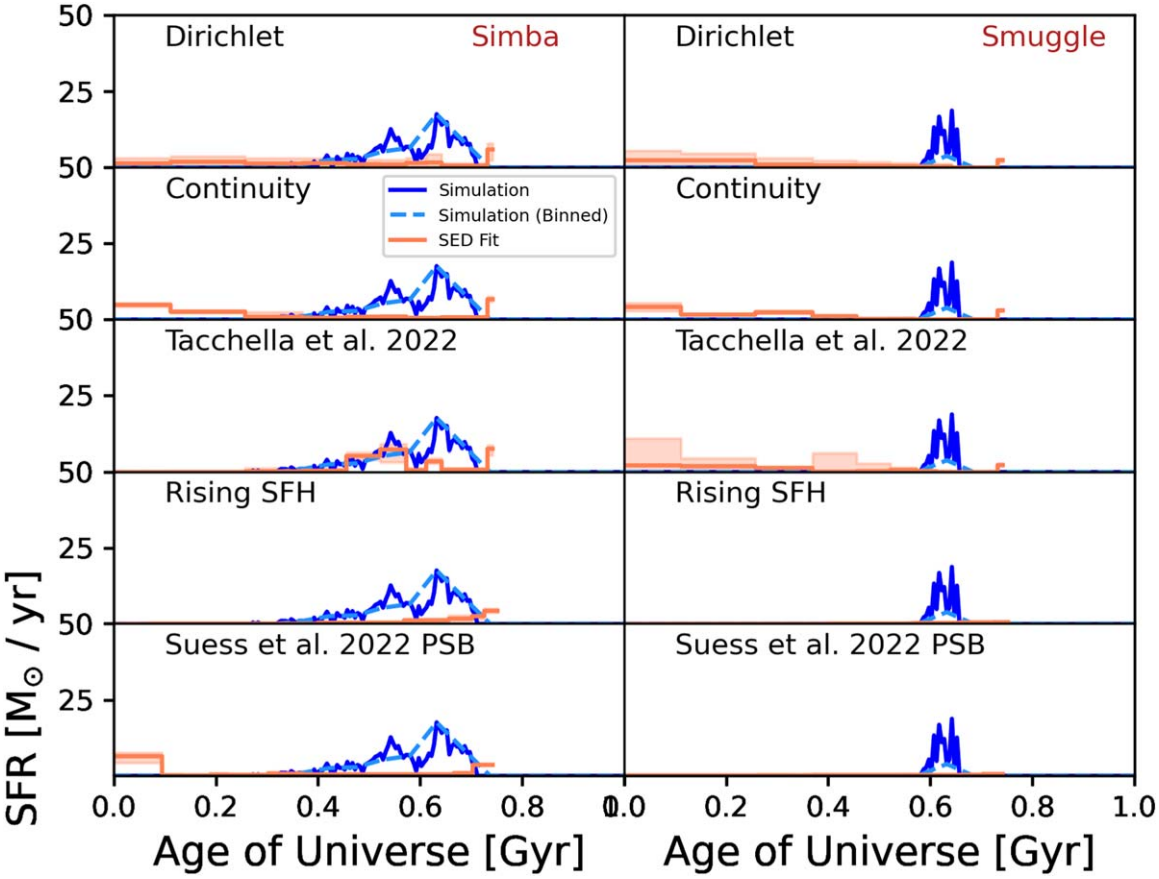

Figure 15. SFHs for the eighth most massive galaxy in the SIMBA (left) and SMUGGLE (right) simulations.

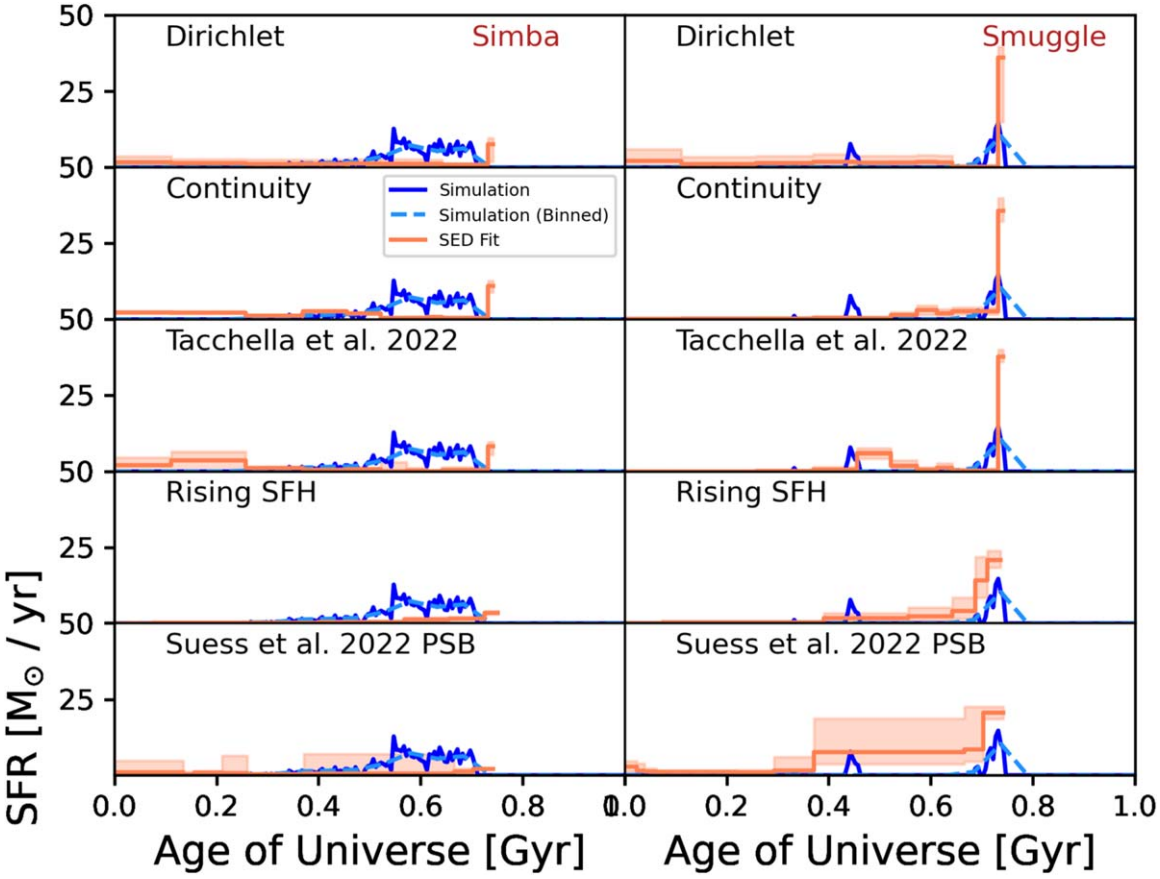

Figure 16. SFHs for the ninth most massive galaxy in the SIMBA (left) and SMUGGLE (right) simulations.

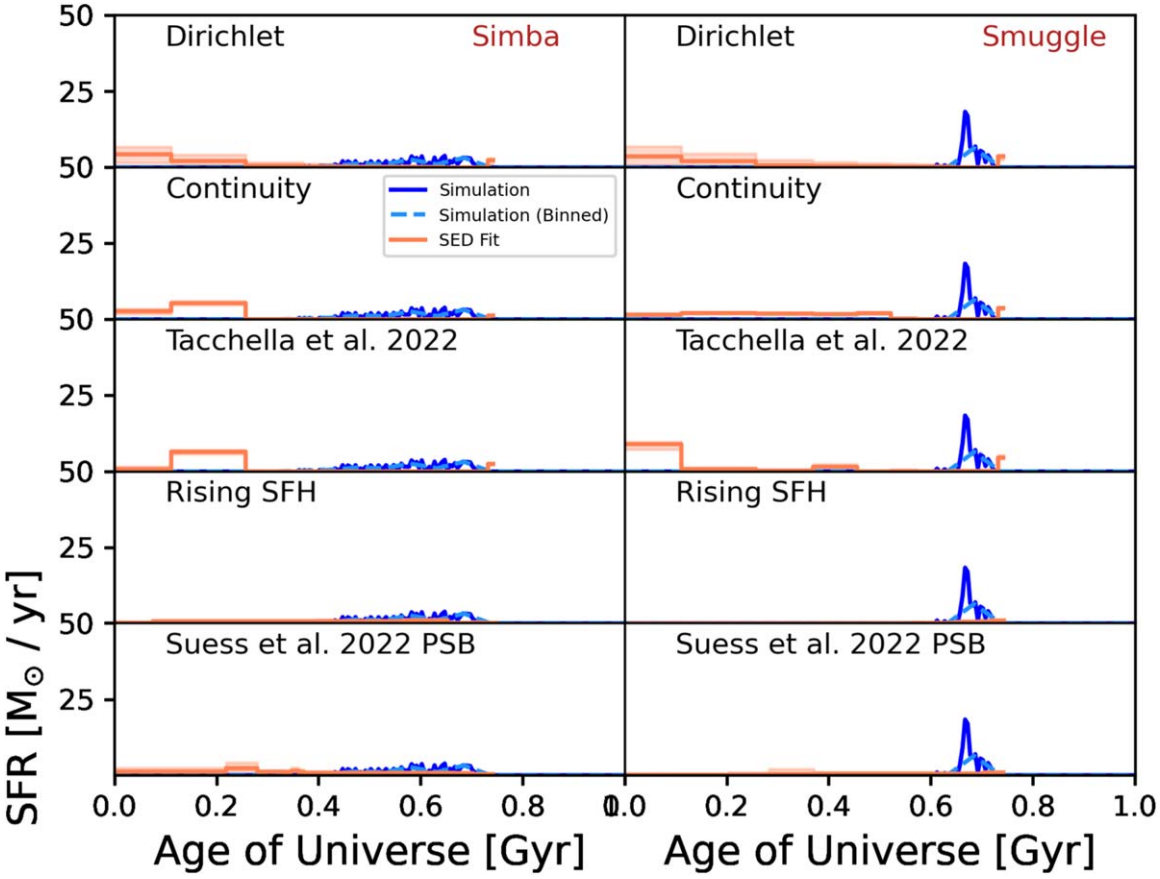

Figure 17. SFHs for the tenth most massive galaxy in the SIMBA (left) and SMUGGLE (right) simulations.

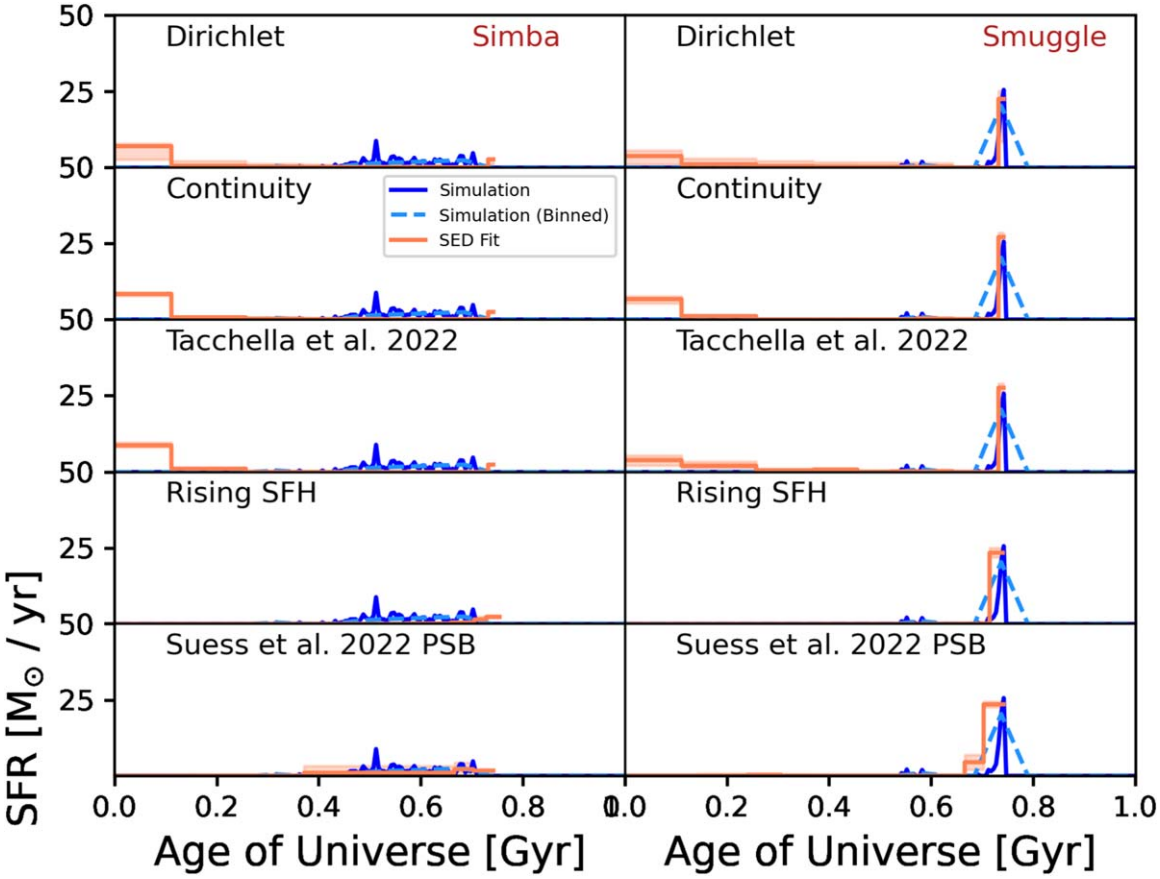

Figure 18. SFHs for the 11th most massive galaxy in the SIMBA (left) and SMUGGLE (right) simulations.

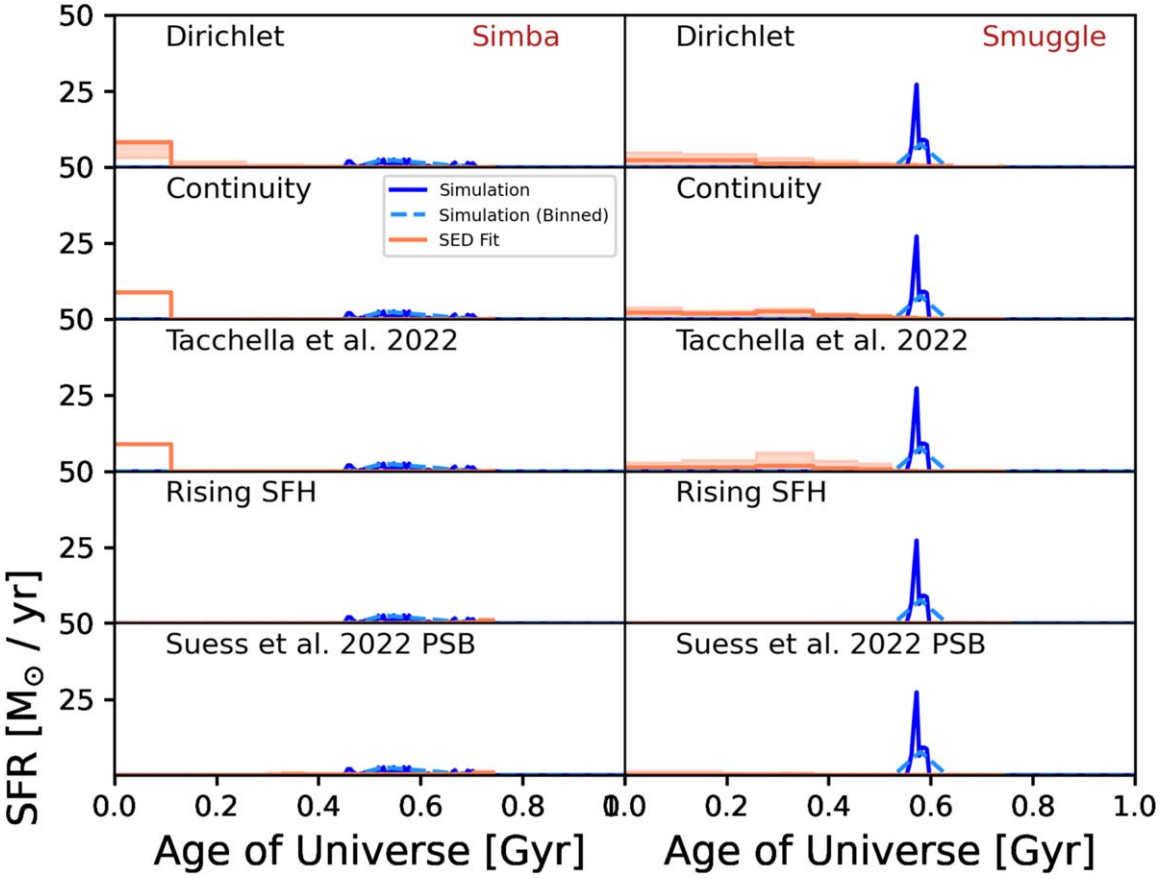

Figure 19. SFHs for the 12th most massive galaxy in the SIMBA (left) and SMUGGLE (right) simulations.

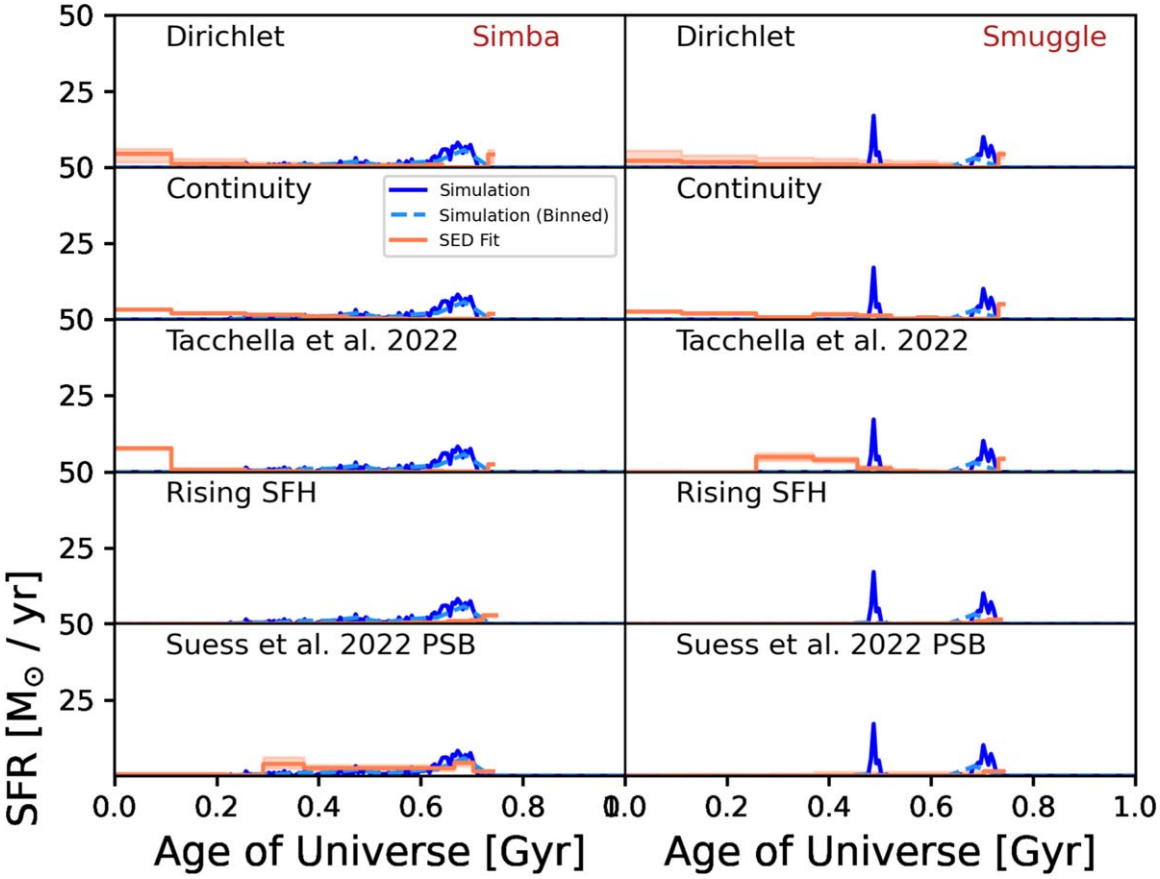

Figure 20. SFHs for the 13th most massive galaxy in the SIMBA (left) and SMUGGLE (right) simulations.

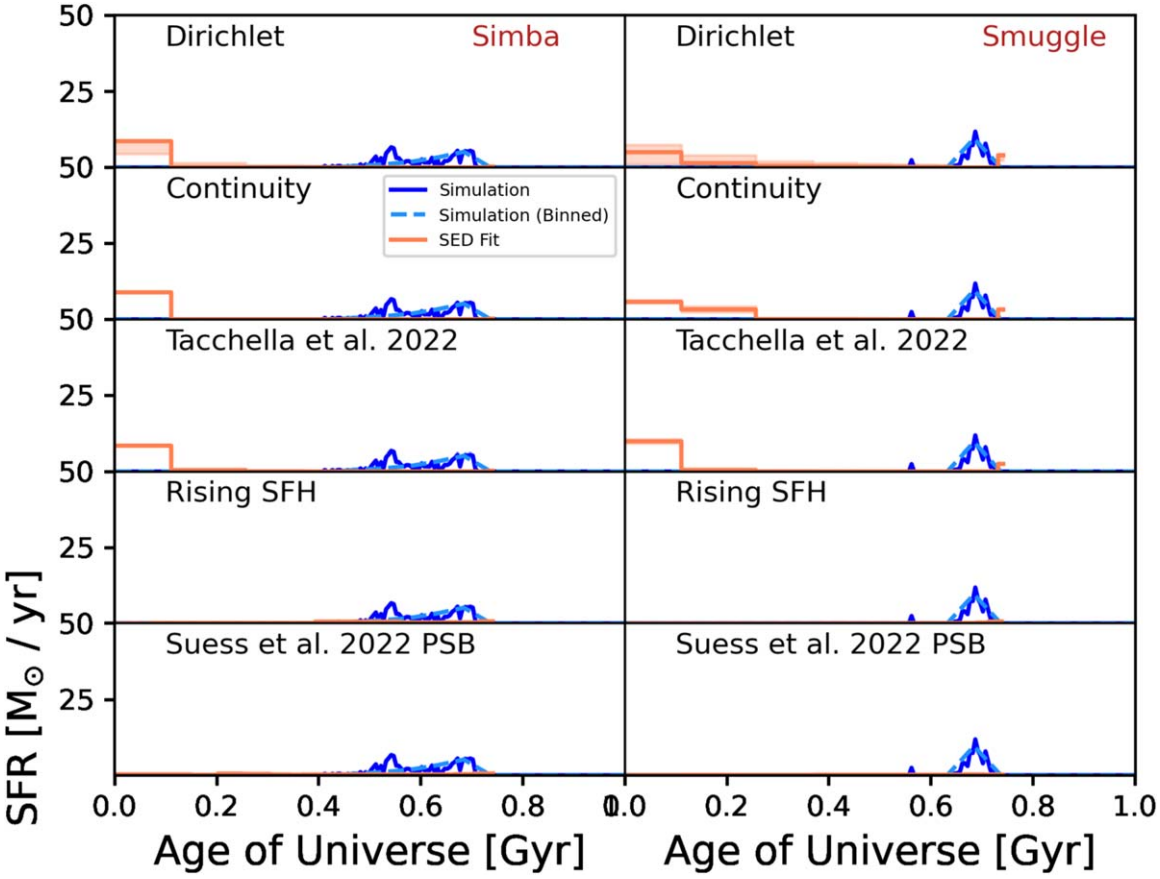

Figure 21. SFHs for the 14th most massive galaxy in the SIMBA (left) and SMUGGLE (right) simulations.

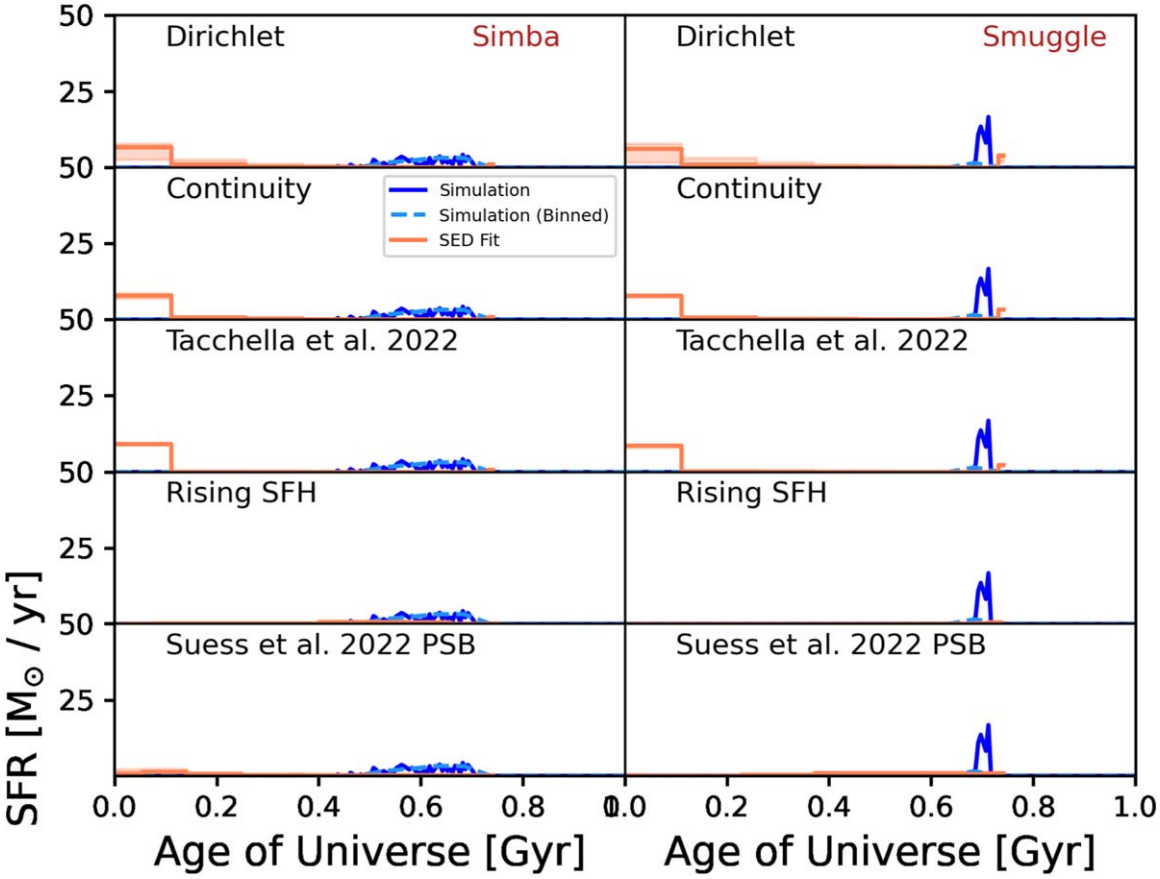

Figure 22. SFHs for the 15th most massive galaxy in the SIMBA (left) and SMUGGLE (right) simulations.

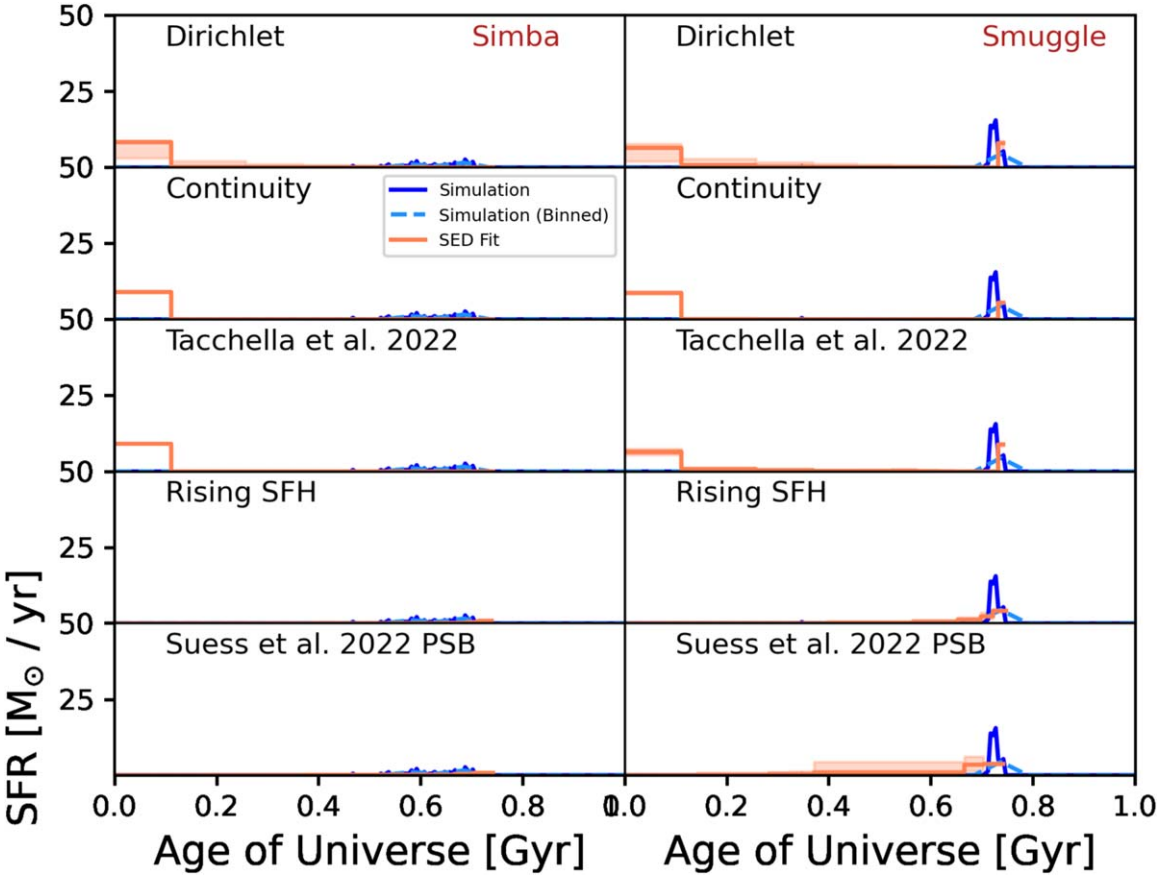

Figure 23. SFHs for the 16th most massive galaxy in the SIMBA (left) and SMUGGLE (right) simulations.

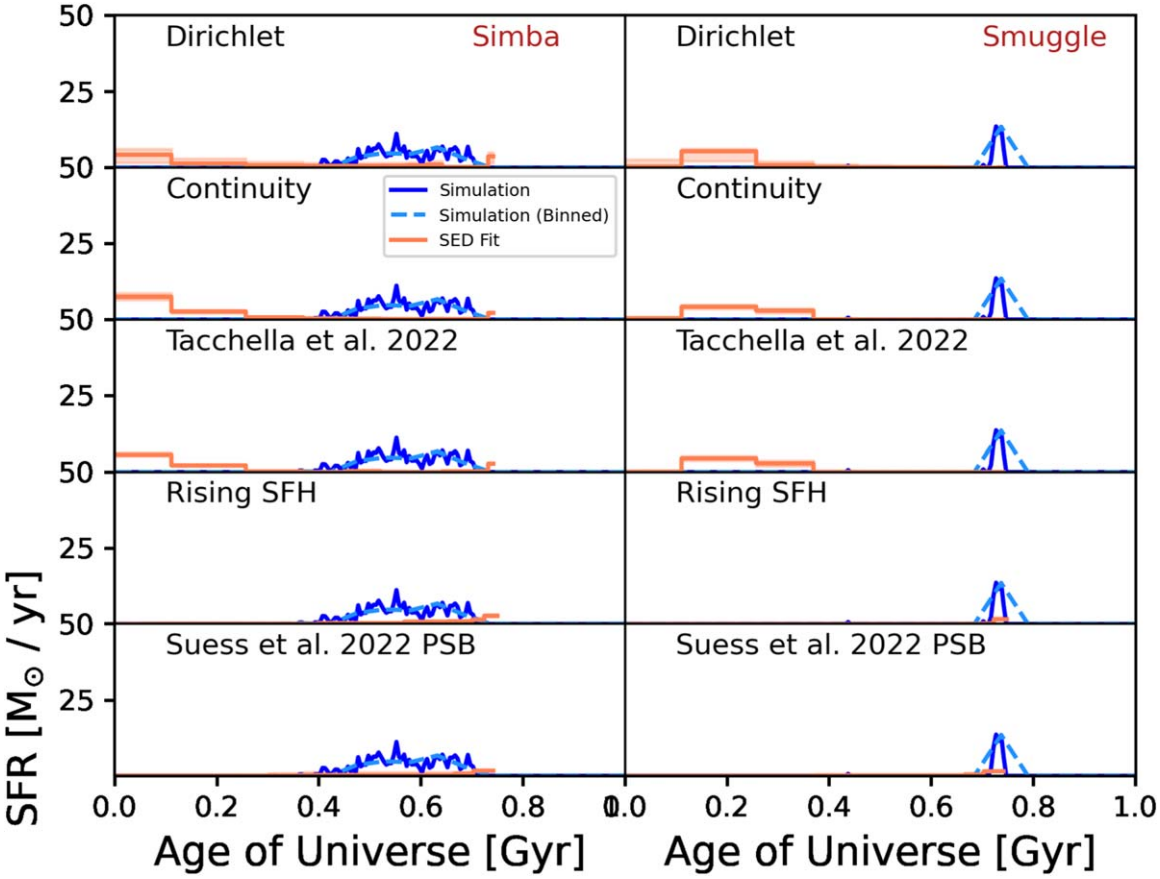

Figure 24. SFHs for the 17th most massive galaxy in the SIMBA (left) and SMUGGLE (right) simulations.

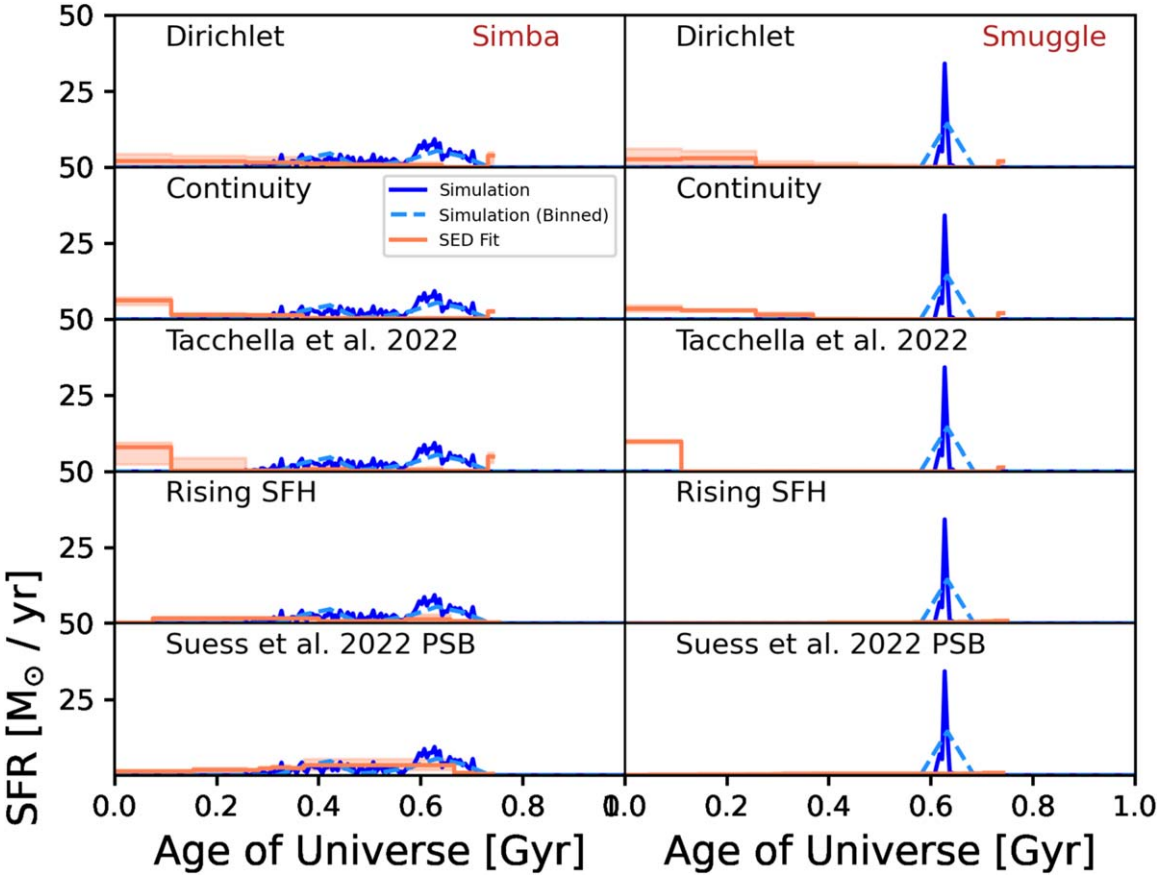

Figure 25. SFHs for the 18th most massive galaxy in the SIMBA (left) and SMUGGLE (right) simulations.

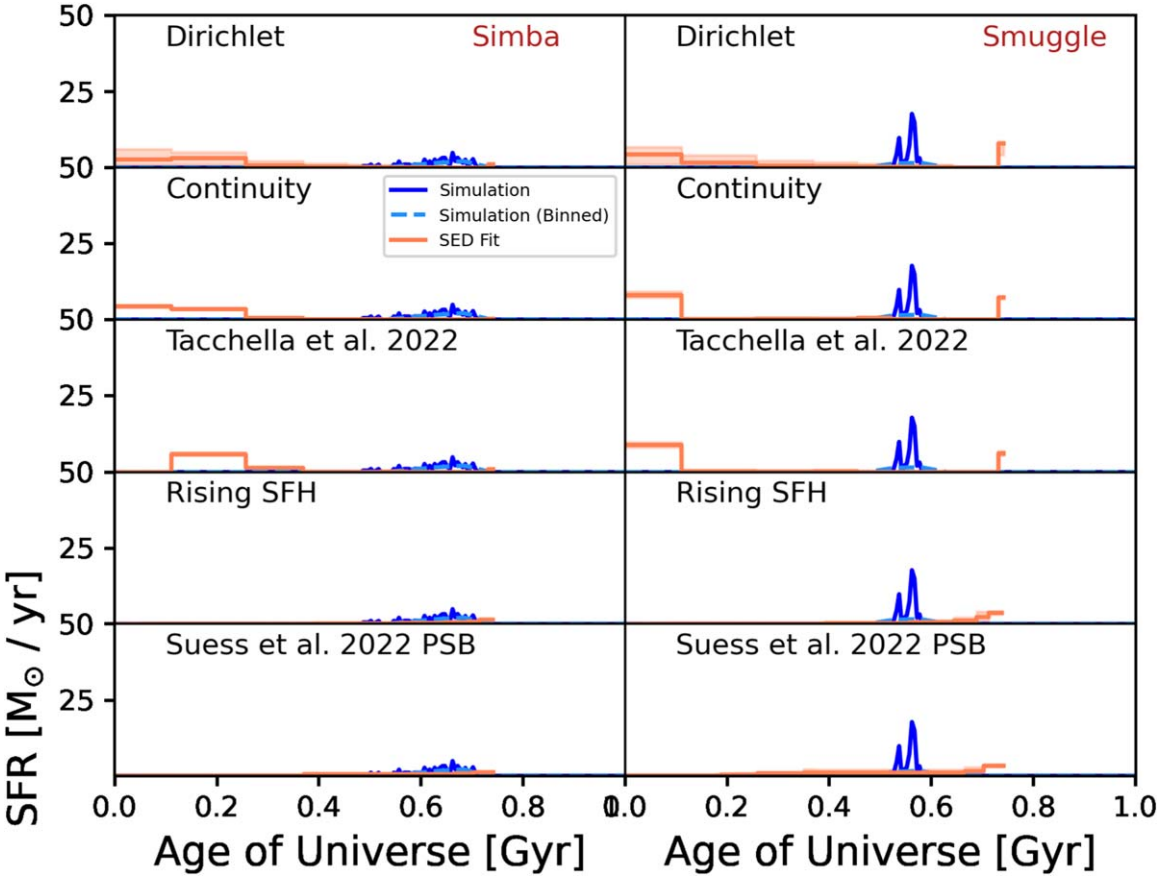

Figure 26. SFHs for the 19th most massive galaxy in the SIMBA (left) and SMUGGLE (right) simulations.

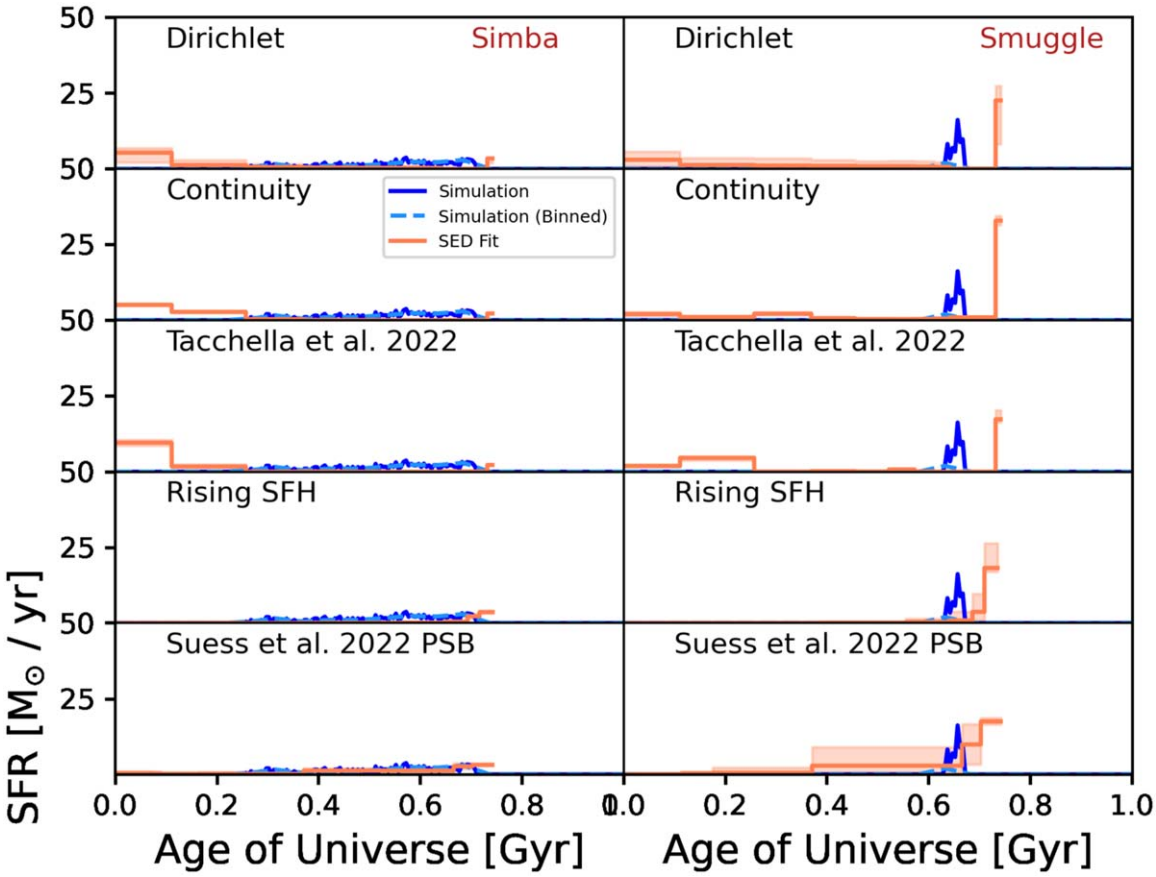

Figure 27. SFHs for the 20th most massive galaxy in the SIMBA (left) and SMUGGLE (right) simulations.

ORCID iDs

Desika Narayanan https://orcid.org/0000-0002-7064-4309
Sidney Lower https://orcid.org/0000-0003-4422-8595
Paul Torrey https://orcid.org/0000-0002-5653-0786
Gabriel Brammer https://orcid.org/0000-0003-2680-005X
Weiguang Cui https://orcid.org/0000-0002-2113-4863
Romeel Davé https://orcid.org/0000-0003-2842-9434
Kartheik G. Iyer https://orcid.org/0000-0001-9298-3523
Qi Li https://orcid.org/0000-0001-8015-2298
Christopher C. Lovell https://orcid.org/0000-0001-7964-5933
Laura V. Sales https://orcid.org/0000-0002-3790-720X
Daniel P. Stark https://orcid.org/0000-0001-6106-5172
Federico Marinacci https://orcid.org/0000-0003-3816-7028
Mark Vogelsberger https://orcid.org/0000-0001-8593-7692

References

Acquaviva, V., Raichoor, A., & Gawiser, E. 2015, ApJ, 804, 8
Adams, N. J., et al. 2023, MNRAS, 518, 4755
Asano, R. S., Takeuchi, T. T., Hirashita, H., & Inoue, A. K. 2013, EP&S, 65, 213
Atek, H., et al. 2023, MNRAS, 519, 1201
Betancourt, M. J., & Girolami, M. 2013, arXiv:1312.0906
Boylan-Kolchin, M. 2023, NatAs, 7, 731
Brammer, G. B., van Dokkum, P. G., & Coppi, P. 2008, ApJ, 686, 1503
Brammer, G. B., et al. 2012, ApJS, 200, 13
Carnall, A. C., Leja, J., Johnson, B. D., et al. 2019, ApJ, 873, 44
Carnall, A. C., McLure, R. J., Dunlop, J. S., & Davé, R. 2018, MNRAS, 480, 4379
Castellano, M., et al. 2022, ApJL, 938, L15
Charlot, S., & Fall, S. M. 2000, ApJ, 539, 718
Chevallard, J., & Charlot, S. 2016, MNRAS, 462, 1415
Choi, J., Dotter, A., Conroy, C., et al. 2016, ApJ, 823, 102
Conroy, C. 2013, ARA&A, 51, 393
Conroy, C., & Gunn, J. E. 2010, ApJ, 712, 833
Conroy, C., Gunn, J. E., & White, M. 2009, ApJ, 699, 486
Conroy, C., & van Dokkum, P. 2012, ApJ, 747, 69
Conroy, C., White, M., & Gunn, J. E. 2010, ApJ, 708, 58
da Cunha, E., Charlot, S., & Elbaz, D. 2008, MNRAS, 388, 1595
Daddi, E., et al. 2004, ApJ, 617, 746
Davé, R. 2008, MNRAS, 385, 147
Davé, R., Anglés-Alcázar, D., Narayanan, D., et al. 2019, arXiv:1901.10203
Davé, R., Rafieferantsoa, M. H., Thompson, R. J., & Hopkins, P. F. 2017, MNRAS, 467, 115
Davé, R., Thompson, R., & Hopkins, P. F. 2016, MNRAS, 462, 3265
Donnan, C. T., et al. 2023, MNRAS, 518, 6011
Draine, B. T., & Lee, H. M. 1984, ApJ, 285, 89
Draine, B. T., Li, A., Hensley, B. S., et al. 2021, ApJ, 917, 3
Dressler, A., et al. 2023, arXiv:2306.02469
Dudzevičiūtė, U., et al. 2020, MNRAS, 494, 3828
Dwek, E. 1998, ApJ, 501, 643
Endsley, R., Stark, D. P., Whitler, L., et al. 2022, arXiv:2208.14999
Endsley, R., et al. 2023, arXiv:2306.05295
Faber, S. M. 1972, A&A, 20, 361
Finkelstein, S. L., Bagley, M., Song, M., et al. 2022a, ApJ, 928, 52
Finkelstein, S. L., Bagley, M. B., Haro, P. A., et al. 2022b, ApJL, 940, L55
Garg, P., et al. 2022, ApJ, 926, 80
Gilda, S., Lower, S., & Narayanan, D. 2021, ApJ, 916, 43
Giménez-Arteaga, C., et al. 2023, ApJ, 948, 126
Graves, G. J., & Faber, S. M. 2010, ApJ, 717, 803
Hahn, O., & Abel, T. 2011, MNRAS, 415, 2101
Harikane, Y., et al. 2023, ApJS, 265, 5
Haslbauer, M., Kroupa, P., Zonoozi, A. H., & Haghi, H. 2022, ApJL, 939, L31
Heavens, A. F., Jimenez, R., & Lahav, O. 2000, MNRAS, 317, 965
Hopkins, P. F. 2015, MNRAS, 450, 53
Hopkins, P. F., Narayanan, D., & Murray, N. 2013, MNRAS, 432, 2647
Iyer, K., & Gawiser, E. 2017, ApJ, 838, 127
Iyer, K. G., Gawiser, E., Faber, S. M., et al. 2019, ApJ, 879, 116

Iyer, K. G., Speagle, J. S., Caplar, N., et al. 2022, arXiv:2208.05938
Iyer, K. G., et al. 2020, MNRAS, 498, 430
Iyer, K., et al. 2018, ApJ, 866, 120
Johnson, B. D., Leja, J., Conroy, C., & Speagle, J. S. 2021, ApJS, 254, 22
Johnson, B. D., Leja, J. L., Conroy, C., & Speagle, J. S., 2019 Prospector: Stellar population inference from spectra and SEDs, Astrophysics Source Code Library, ascl:1905.025
Kennicutt, R. C., Jr 1998, ARA&A, 36, 189
Kriek, M., van Dokkum, P. G., Labbé, I., et al. 2009, ApJ, 700, 221
Kroupa, P. 2002, Sci, 295, 82
Krumholz, M. R., McKee, C. F., & Tumlinson, J. 2009, ApJ, 693, 216
Labbé, I., et al. 2023, Natur, 616, 266
Laor, A., & Draine, B. T. 1993, ApJ, 402, 441
Leja, J., Carnall, A. C., Johnson, B. D., Conroy, C., & Speagle, J. S. 2019a, ApJ, 876, 3
Leja, J., Johnson, B. D., Conroy, C., van Dokkum, P. G., & Byler, N. 2017, ApJ, 837, 170
Leja, J., Johnson, B. D., Conroy, C., et al. 2019b, ApJ, 877, 140
Li, Q., Narayanan, D., & Davé, R. 2019, MNRAS, 490, 1425
Li, Q., Narayanan, D., Torrey, P., Davé, R., & Vogelsberger, M. 2021, MNRAS, 507, 548
Lovell, C. C., Acquaviva, V., & Thomas, P. A. 2019, MNRAS, 490, 5503
Lower, S., Narayanan, D., Leja, J., et al. 2020, ApJ, 904, 33
Lower, S., Narayanan, D., Leja, J., et al. 2022, ApJ, 931, 14
Madau, P., & Dickinson, M. 2014, ARA&A, 52, 415
Maraston, C., Pforr, J., & Renzini, A. 2010, MNRAS, 407, 830
Marinacci, F., Sales, L. V., Vogelsberger, M., Torrey, P., & Springel, V. 2019, MNRAS, 489, 4233
Mason, C. A., Trenti, M., & Treu, T. 2023, MNRAS, 521, 497
McKinnon, R., Torrey, P., Vogelsberger, M., Hayward, C. C., & Marinacci, F. 2017, MNRAS, 468, 1505
Michalowski, M. J., Dunlop, J. S., Cirasuolo, M., et al. 2012, A&A, 541, A85
Naidu, R. P., et al. 2022, ApJL, 940, L14
Narayanan, D., Conroy, C., Davé, R., Johnson, B. D., & Popping, G. 2018, ApJ, 869, 70
Narayanan, D., et al. 2021, ApJS, 252, 12
Narayanan, D., et al. 2023, arXiv:2301.07136
Pacifici, C., et al. 2023, ApJ, 944, 141
Papovich, C., Dickinson, M., & Ferguson, H. C. 2001, ApJ, 559, 620
Pforr, J., Maraston, C., & Tonini, C. 2013, MNRAS, 435, 1389
Popping, G., Puglisi, A., & Norman, C. A. 2017, MNRAS, 472, 2315
Robertson, B. E., et al. 2023, NatAs, 7, 611
Robitaille, T. P. 2011, A&A, 536, A79
Salim, S., & Narayanan, D. 2020, ARA&A, 58, 529
Shapley, A. E., Steidel, C. C., Adelberger, K. L., et al. 2001, ApJ, 562, 95
Shapley, A. E., Steidel, C. C., Erb, D. K., et al. 2005, ApJ, 626, 698
Shen, X., Vogelsberger, M., Boylan-Kolchin, M., Tacchella, S., & Kannan, R. 2023, MNRAS, 525, 3254
Simha, V., Weinberg, D. H., Conroy, C., et al. 2014, arXiv:1404.0402
Skelton, R. E., et al. 2014, ApJS, 214, 24
Smith, B. D., et al. 2017, MNRAS, 466, 2217
Sorba, R., & Sawicki, M. 2018, MNRAS, 476, 1532
Sparre, M., Hayward, C. C., & Feldmann, R. 2017, MNRAS, 466, 88
Spinrad, H., & Taylor, B. J. 1971, ApJS, 22, 445
Springel, V. 2010, MNRAS, 401, 791
Stark, D. P., Schenker, M. A., Ellis, R., et al. 2013, ApJ, 763, 129
Suess, K. A., et al. 2022, ApJ, 935, 146
Tacchella, S., et al. 2022, ApJ, 927, 170
Tinsley, B. M. 1968, ApJ, 151, 547
Tojeiro, R., Heavens, A. F., Jimenez, R., & Panter, B. 2007, MNRAS, 381, 1252
Topping, M. W., et al. 2022, MNRAS, 516, 975
Trager, S. C., Faber, S. M., & Dressler, A. 2008, MNRAS, 386, 715
Trayford, J. W., Lagos, C. d. P., Robotham, A. S. G., & Obreschkow, D. 2020, MNRAS, 491, 3937
Tsai, J. C., & Mathews, W. G. 1995, ApJ, 448, 84
Turk, M. J., Smith, B. D., Oishi, J. S., et al. 2011, ApJS, 192, 9
van Dokkum, P. G. 2008, ApJ, 674, 29
Walcher, J., Groves, B., Budavári, T., & Dale, D. 2011, Ap&SS, 331, 1
Wang, B., Leja, J., Bezanson, R., et al. 2023, ApJL, 944, L58
Weinberger, R., Springel, V., & Pakmor, R. 2020, ApJS, 248, 32
Weingartner, J. C., & Draine, B. T. 2001, ApJ, 548, 296
Whitler, L., Endsley, R., & Stark, D. P. 2023, MNRAS, 519, 157